AMERICAN SOCIETY FOR MICROBIOLOGY | mBio®

RESEARCH ARTICLE
Molecular Biology and Physiology

A Grad-seq View of RNA and Protein Complexes in *Pseudomonas aeruginosa* under Standard and Bacteriophage Predation Conditions

Milan Gerovac,[a] Laura Wicke,[a,b] Kotaro Chihara,[c] Cornelius Schneider,[a,d] Rob Lavigne,[b] Jörg Vogel[a,c]

[a]Institute for Molecular Infection Biology (IMIB), University of Würzburg, Würzburg, Germany
[b]Laboratory of Gene Technology, KU Leuven, Leuven, Belgium
[c]Helmholtz Institute for RNA-based Infection Research (HIRI), Helmholtz Centre for Infection Research (HZI), Würzburg, Germany
[d]Department of Biochemistry and Cancer Therapy Research Center (CTRC), Theodor Boveri-Institute, University of Würzburg, Würzburg, Germany

ABSTRACT The Gram-negative rod-shaped bacterium *Pseudomonas aeruginosa* is not only a major cause of nosocomial infections but also serves as a model species of bacterial RNA biology. While its transcriptome architecture and posttranscriptional regulation through the RNA-binding proteins Hfq, RsmA, and RsmN have been studied in detail, global information about stable RNA-protein complexes in this human pathogen is currently lacking. Here, we implement gradient profiling by sequencing (Grad-seq) in exponentially growing *P. aeruginosa* cells to comprehensively predict RNA and protein complexes, based on glycerol gradient sedimentation profiles of >73% of all transcripts and ~40% of all proteins. As to benchmarking, our global profiles readily reported complexes of stable RNAs of *P. aeruginosa*, including 6S RNA with RNA polymerase and associated product RNAs (pRNAs). We observe specific clusters of noncoding RNAs, which correlate with Hfq and RsmA/N, and provide a first hint that *P. aeruginosa* expresses a ProQ-like FinO domain-containing RNA-binding protein. To understand how biological stress may perturb cellular RNA/protein complexes, we performed Grad-seq after infection by the bacteriophage ΦKZ. This model phage, which has a well-defined transcription profile during host takeover, displayed efficient translational utilization of phage mRNAs and tRNAs, as evident from their increased cosedimentation with ribosomal subunits. Additionally, Grad-seq experimentally determines previously overlooked phage-encoded noncoding RNAs. Taken together, the *Pseudomonas* protein and RNA complex data provided here will pave the way to a better understanding of RNA-protein interactions during viral predation of the bacterial cell.

IMPORTANCE Stable complexes by cellular proteins and RNA molecules lie at the heart of gene regulation and physiology in any bacterium of interest. It is therefore crucial to globally determine these complexes in order to identify and characterize new molecular players and regulation mechanisms. Pseudomonads harbor some of the largest genomes known in bacteria, encoding ~5,500 different proteins. Here, we provide a first glimpse on which proteins and cellular transcripts form stable complexes in the human pathogen *Pseudomonas aeruginosa*. We additionally performed this analysis with bacteria subjected to the important and frequently encountered biological stress of a bacteriophage infection. We identified several molecules with established roles in a variety of cellular pathways, which were affected by the phage and can now be explored for their role during phage infection. Most importantly, we observed strong colocalization of phage transcripts and host ribosomes, indicating the existence of specialized translation mechanisms during phage infection. All data are publicly available in an interactive and easy to use browser.

Citation Gerovac M, Wicke L, Chihara K, Schneider C, Lavigne R, Vogel J. 2021. A Grad-seq view of RNA and protein complexes in *Pseudomonas aeruginosa* under standard and bacteriophage predation conditions. mBio 12:e03454-20. https://doi.org/10.1128/mBio.03454-20.

Editor Edward G. Ruby, University of Hawaii at Manoa

Address correspondence to Rob Lavigne, rob.lavigne@kuleuven.be, or Jörg Vogel, joerg.vogel@uni-wuerzburg.de.

This article is a direct contribution from Jörg Vogel, a Fellow of the American Academy of Microbiology, who arranged for and secured reviews by Udo Bläsi, Max F. Perutz Laboratories, University of Vienna, and Rotem Sorek, Weizmann Institute of Science.

Received 7 December 2020
Accepted 16 December 2020
Published 9 February 2021

KEYWORDS Grad-seq, *Pseudomonas*, ΦKZ, bacteriophage, infection, *Pseudomonas aeruginosa*, RNA-binding proteins, noncoding RNA, phage

Pseudomonas aeruginosa is a Gram-negative environmental gammaproteobacterium and a critical life-threatening pathogen in humans with compromised immune defense (1). It is the main cause of death in cystic fibrosis patients (2) and is hard to treat with antibiotics due to its diverse export capabilities and its ability to form strong biofilms (3). Unsurprisingly, the medical challenges associated with nosocomial infections and drug resistance of *P. aeruginosa* have prompted much effort to better understand the molecular biology of this important human pathogen. With a size of 6.3 Mbp and ~5,570 predicted open reading frames (ORFs), the genome of *P. aeruginosa* is one of the largest among prokaryotes (4). These genes, many of which encode paralogous proteins, endow the bacterium with a remarkable functional diversity that allows it to thrive in different habitats. Gene expression control also seems to be complex in *P. aeruginosa*: an unusually high 8.4% of all genes are predicted to encode regulatory proteins, foremost, transcription factors.

In addition to extensive gene regulation at the DNA level, there has been increasing evidence for posttranscriptional regulation to play an important role in *P. aeruginosa* (5). The bacterium possesses homologs of two general RNA-binding proteins (RBPs), CsrA and Hfq, which work in conjunction with small regulatory RNAs (6). An important role of Hfq in *P. aeruginosa* was first predicted almost 15 years ago when an *hfq* knockout strain was observed to display altered levels for 5% of all transcripts (7). More recent work employing global RNA interactome techniques (8–11) suggests that Hfq interacts with a large number of coding and noncoding transcripts of *P. aeruginosa*. A distinct feature of Hfq-mediated regulation in *Pseudomonas* is that Hfq inhibits translation of target transcripts by forming a regulatory complex with the catabolite repression protein Crc (12, 13), likely by recognition of nascent transcripts (9).

The other major regulatory RBPs include the CsrA-like proteins RsmA and RsmN, which act as global translational repressors through recognizing GGA motifs in the 5′ region of mRNAs (14–18), partly so in a combinatorial fashion with Hfq (19). In contrast, much less is known about a putative homolog of FinO/ProQ-like proteins, which is an emerging new family of small regulatory RNA (sRNA)-related RBPs in Gram-negative bacteria (20–24). Judging by the presence of a FinO domain, *P. aeruginosa* does possess a candidate protein (25), but whether it is expressed and forms complexes with cellular transcripts remains unknown. Similarly, cold shock proteins (CSPs), which interact with hundreds if not thousands of transcripts in some bacteria (26), have not been studied in *P. aeruginosa*.

The past couple of years have witnessed the development of new methods to discover RBPs and study RNA-protein complexes and interactions on a global level (27), one of which is gradient profiling by sequencing, also known as Grad-seq (22). Grad-seq partitions native cellular lysates, including RNA-protein complexes, on a glycerol gradient according to their molecular weight and shape. Subsequent fractionation and analysis by transcriptome sequencing (RNA-seq) and mass spectrometry of each fraction enables visualization of in-gradient distributions of, ideally, all expressed RNAs and detectable soluble proteins from the growth condition of interest. The method has been successfully applied to several different bacteria, revealing in *Salmonella enterica* a previously unknown global activity of ProQ (22), new stable RNA and protein associations with the ribosome in *Escherichia coli* (28), and a mechanism of sRNA stabilization by 3′→5′ exonucleolytic trimming in the Gram-positive human pathogen *Streptococcus pneumoniae* (29). In all these studies, Grad-seq produced a previously unavailable resource for the comprehensive prediction of protein complexes, with or without RNA components, of a wide functional spectrum.

Despite its importance as a human pathogen and model bacterium, global data informing on RNA/protein complexes are lacking for *P. aeruginosa* as well as other pseudomonads. Here, we pioneer the application of bacterial complexomics in *P.*

aeruginosa, analyzing exponentially growing cultures of this bacterium with Grad-seq. Our analysis provides the first systems biology-based description of RNA-based housekeeping and regulatory systems in this species, which includes a stable RNA polymerase (RNAP)-6S RNA complex. We describe in-gradient distribution for thousands of mRNAs and sRNAs and predict hundreds of protein complexes involving metabolic and signal transduction proteins. In addition to performing Grad-seq on naive bacteria, we apply the approach for the first time to visualize transcript associations of an invading phage (ΦKZ) and to identify phage-encoded regulatory RNAs. These data sets are provided along with an online browser that helps to visualize the obtained sedimentation profiles in a searchable fashion and allows for them to be compared with Grad-seq data from other Gram-negative and Gram-positive species.

RESULTS

Gradient fractionation of *P. aeruginosa* in early exponential growth phase. As a prerequisite for Grad-seq of *P. aeruginosa* (see workflow in Fig. 1A), we established a glycerol gradient analysis of RNA and proteins from a lysate of strain PAO1. We chose to analyze samples from the exponential phase of growth (optical density at 600 nm [OD_{600}] of 0.3) in a rich culture medium to allow comparisons to previously established analyses under standard growth conditions. In addition, the exponential phase is optimal for phage infection and replication of ΦKZ (30). Phage predation represents a biotic stress for PAO1, relevant to the experimental design and narrative below. A cleared lysate was separated on a 10% to 40% glycerol gradient, followed by fractionation and gel-based analysis of either protein or RNA molecules in each of the 20 fractions obtained. In addition, the pellet was included in this analysis, as it contains translating ribosomes as well as aggregated and unfolded proteins.

As a quality control, we determined the absorption profile of the gradient fractions at 260 nm (Fig. 1B). We observed the expected bulk peak at the top of the gradient, which corresponds to free proteins and RNAs in low-molecular-weight (LMW) fractions. Also, two pronounced peaks corresponding to the small (30S) and large (50S) ribosomal subunits in high-molecular-weight (HMW) fractions were observed. Compared to previously obtained profiles for Grad-seq of *E. coli* or *S. enterica* (22, 28), we observed many fewer 70S ribosomes. In addition, the ribosomal subunits were shifted by one fraction toward the top of the gradient, which might indicate species-specific disintegration of ribosomal subunit complexes or a relaxed rRNA configuration in *Pseudomonas* under the present growth condition.

SDS-PAGE showed general distributions of abundant soluble proteins and their complexes within the gradient (Fig. 1C). As expected, translation factor EF-Tu is one of the most abundant proteins in *Pseudomonas* (see Table S1 and Fig. S2B and C in the supplemental material). The EF-Tu protein, which transiently delivers tRNAs to the ribosome (31), primarily sedimented in a ribosome-free manner, occurring in the LMW fractions 1 to 3. RNAP subunits were primarily found in fractions 5 to 7, whereas the major protein GroEL abounded in fractions 6 to 9 (i.e., complexes in the ~400- to 800-kDa range). The 30S and 50S ribosomal subunits, with a molecular weight of ~1 MDa and ~2 MDa, respectively, sedimented in fractions 9 to 13 or 14 to 16.

Similarly, we stained abundant RNA molecules in the individual gradient fractions separated in a denaturing gel (Fig. 1D). As expected, tRNAs sedimented primarily in LMW fractions 1 to 4, whereas the abundant 16S and 23S/5S rRNA molecules coincided with the 30S or 50S proteins in fractions 9 to 13 or 14 to 17, respectively. As a benchmark, we also determined the sedimentation profiles of several stable RNAs by Northern blotting analysis (Fig. 1E). Transfer/mRNA (tmRNA; encoded by *ssrA*) forms a ribonucleoprotein particle (RNP) with the SmpB protein to rescue stalled ribosome by a *trans*-translation mechanism (32). Consistent with previous studies in *E. coli* and *S. enterica*, tmRNA sedimented in fractions 3 to 7 (22, 28). The 180-nucleotide (nt) 6S RNA (33) accumulated in fractions 5 to 7, as expected from its reported association with RNAP in *E. coli* (34). In summary, these observations qualified the gradient samples for high-throughput analysis by Grad-seq,

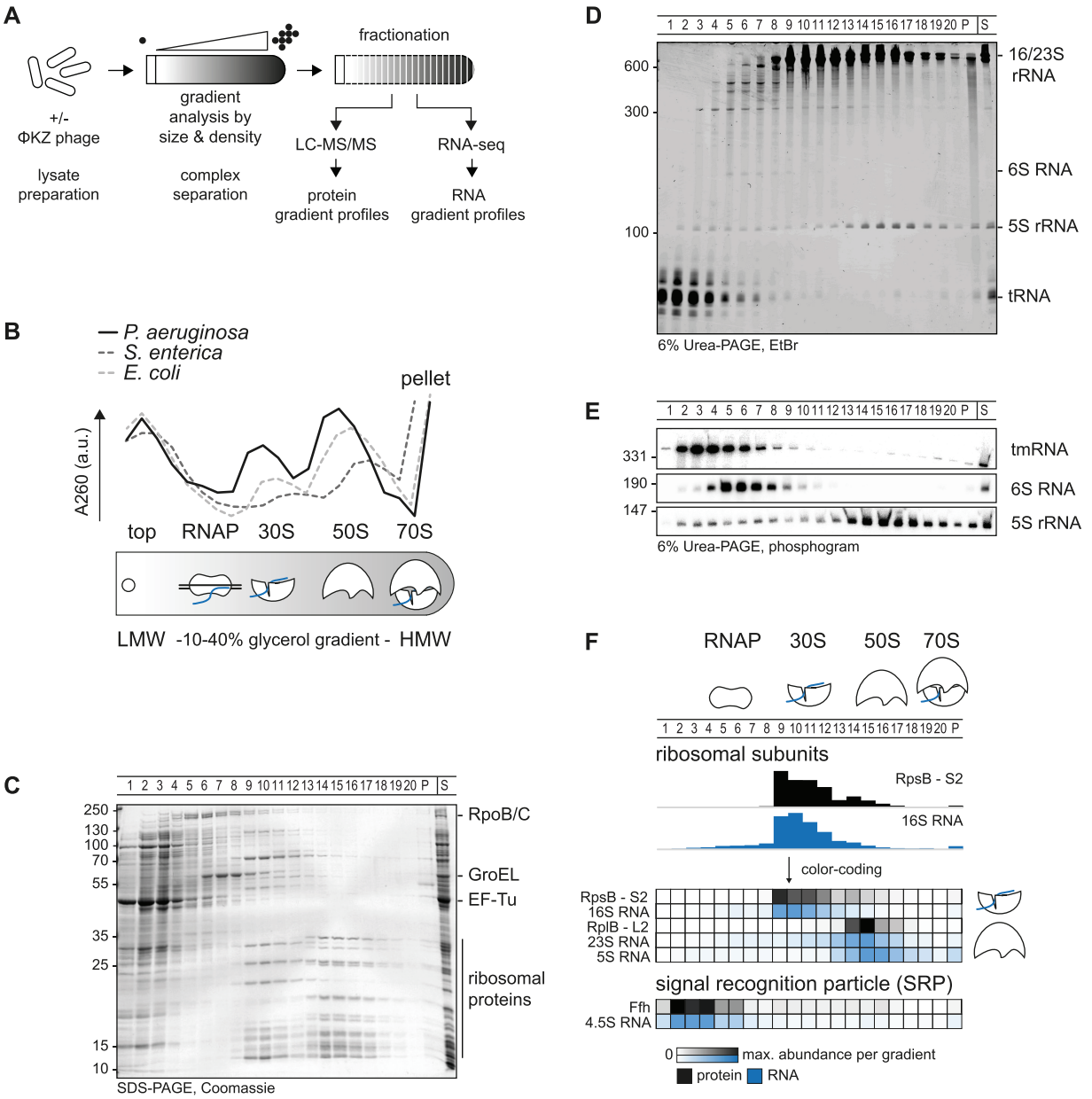

FIG 1 Grad-seq in *Pseudomonas*. (A) Cellular lysate is analyzed in a gradient and fractionated. High-throughput analysis by mass-spectrometry (LC-MS/MS) and RNA-sequencing reveal sedimentation profiles. (B) Complexes are resolved in a 10% to 40% glycerol gradient by size and density. The 260-nm absorption profile of *Pseudomonas* lysate indicates LMW fractions at the top, 30S small, 50S large ribosomal subunits at fractions 9 and 15, respectively, and an elevated absorption in the pellet at HMW fractions. The profile is shifted by approximately one fraction compared to those for *E. coli* and *S. enterica*. The RNAP sediments between the top and 30S subunit. (C) The apparent proteome resembles the positions in panel B. EF-Tu is a transient translation factor and sedimented in the top; RNAP subunits RpoB/C and GroEL sediment before 30S fractions. (D) tRNAs sedimented in top fractions, ribosomal RNAs resemble well the distribution in panels B and C, and 6S RNA sedimentation correlated with RNAP in panel C. (E) tmRNA sedimented in the pellet and at RNAP fractions; 6S RNA sedimentation correlated with RNAP fractions and 5S rRNA with 50S ribosomal subunit fractions. (F) High-throughput-determined sedimentation profiles matched well with in-gel and previously published results in other species.

with the aim to obtain global sedimentation profiles of cellular RNA and protein molecules (Fig. 1F).

Global predictions of macromolecular complexes for *P. aeruginosa*. For a global view of stable complexes in the exponential growth phase, we profiled the proteins and transcripts from each gradient fraction by mass spectrometry and RNA-seq, respectively (Table S1). Protein and RNA abundance was normalized using external spike-ins, enabling us to delimit the detection thresholds (see Fig. S1). Targeted

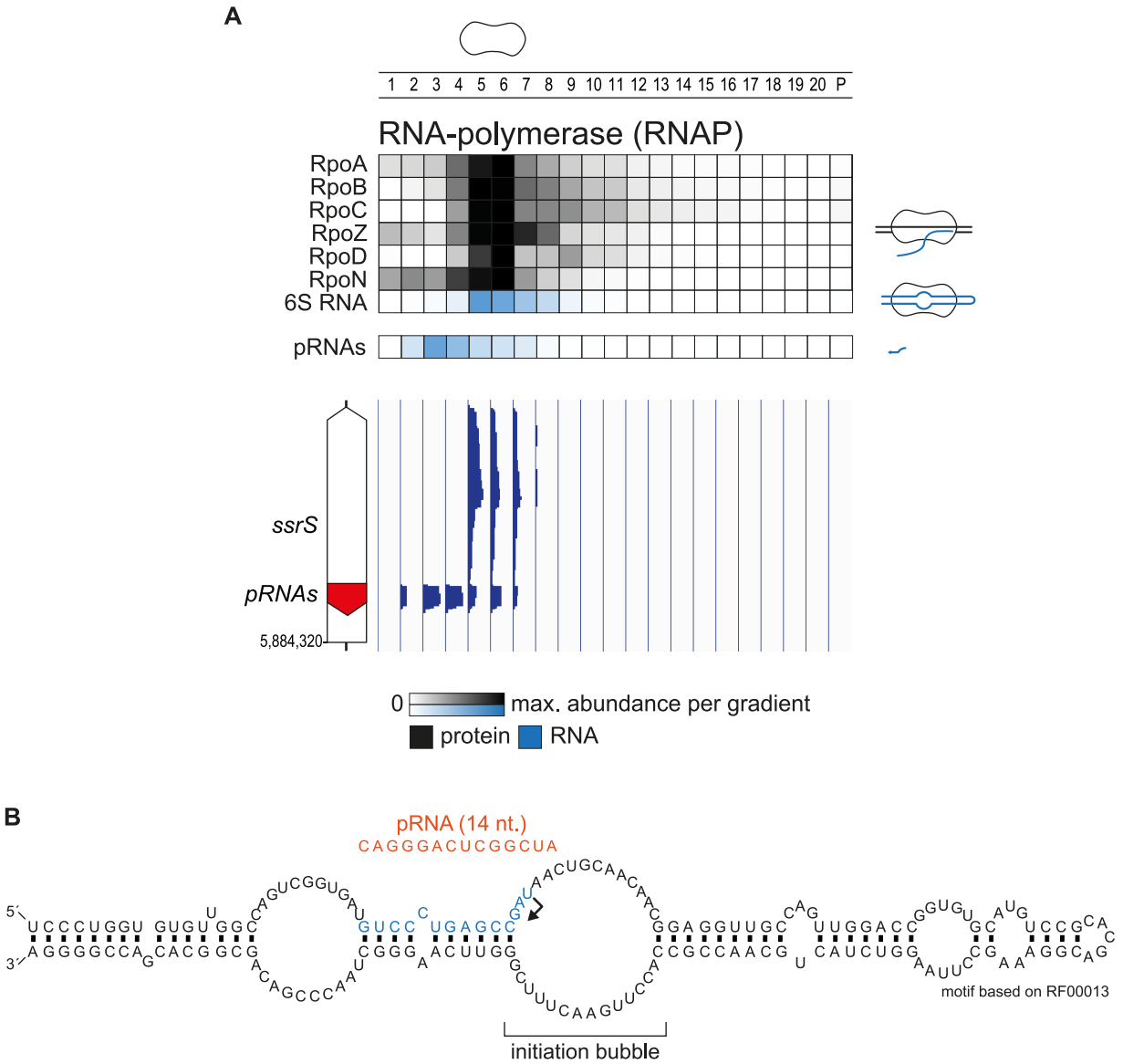

FIG 2 Grad-seq allows for mapping of pRNAs. (A) RNAP subunits, 6S RNA and pRNAs cosedimented in the gradient. pRNAs were mapped by differential sedimentation. Importantly, pRNAs sedimented at a much larger position in fraction three, indicating presence in a complex. (B) The precise position of pRNAs transcription initiation in the 6S initiation bubble was mapped based on differential read coverage from panel A. The structure of 6S RNA was mapped based on the Rfam annotation RF00013.

inspection of these high-throughput data readily showed expected co-occurrences of stable RNA species with their major protein partners (Fig. 1F; see also Fig. S2). For example, cDNA counts of the 16S/23S rRNAs peaked in the same fractions as for peptide counts of the respective ribosomal proteins, and 4.5S RNA of the signal recognition particle (SRP) peaked in the same fractions as for the major SRP protein Ffh. Another case in point is the 6S RNA-RNAP complex whose protein components (RpoA/B/C/Z encoding the $\alpha/\beta/\beta'/\omega$ subunits of RNAP) aligned well with 6S RNA in gradient fractions 5 and 6 (Fig. 2A). Grad-seq even recovered the tiny product RNAs (pRNAs) (35, 36) produced by RNAP as it disentangles itself from the 6S RNA (Fig. 2B). These established interactions provide additional confidence to the correlations described below. Mass spectrometry recovered 2,182 proteins in total, i.e., ~40% of the annotated proteome of *P. aeruginosa* strain PAO1 (37), with these proteins showing a wide range of distribution in the gradient (Fig. 3A and S2A). While most of these proteins sedimented

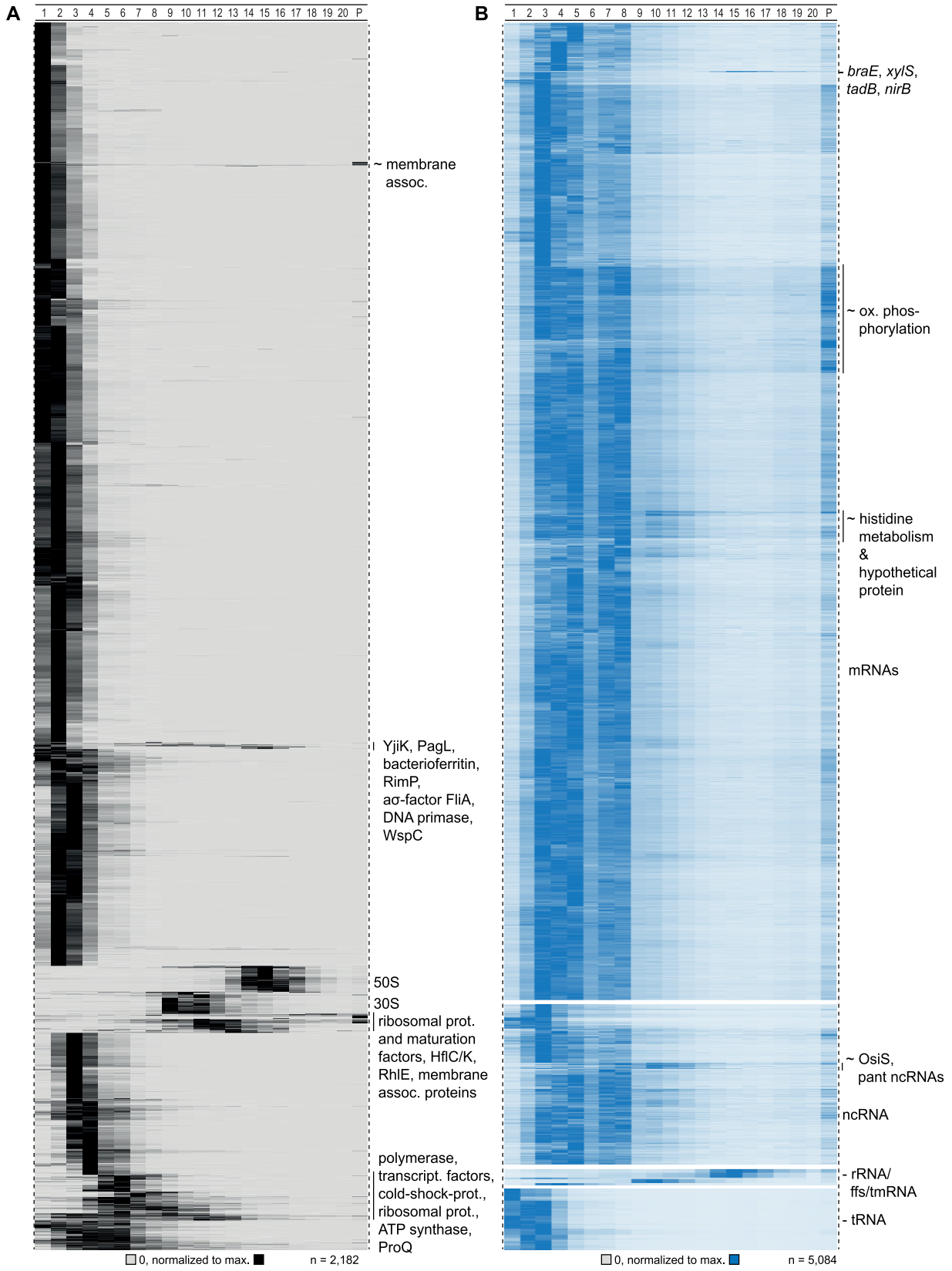

FIG 3 Detected sedimentation profiles in Grad-seq. (A) Proteins sedimented mainly in the first couple of fractions. Defined clusters appeared in fraction below 10. Ribosomal proteins sedimented around fractions 10 and 16. (B) Transcripts (merged CDS and UTRs) sedimented mainly in RNAP and ribosomal fractions. tRNAs did not enter the gradient, and ribosomal RNAs were allocated to HMW fractions.

in LMW fractions 1 to 3, indicating that they are part of either no or only small complexes, there were also protein clusters in the HMW fractions, in addition to the expected two ribosomal subunit clusters. We will return to some of these HMW clusters in the next section.

Viewing the RNA-seq results from individual fractions (Fig. 3B), we observed the expected sedimentation of rRNAs in the HMW part of the gradient, whereas tRNAs were found in the LMW top fractions, both of which recapitulated the preceding gel analysis (Fig. 1D). However, most of the 5,084 transcripts detected in total sedimented in the first eight fractions, and this equally applied to mRNAs and noncoding RNAs (ncRNAs). With respect to mRNAs, this implies that most of these reads stem from transcripts that are not undergoing translation. However, there is a group of mRNAs with abundant reads in the pellet, indicating association with 70S ribosomes or even polysomes. These transcripts show enrichment for functions in oxidative phosphorylation, the tricarboxylic acid (TCA) cycle, and other metabolic pathways. In essence, these sedimentation profiles provide a glimpse of translational utilization of cellular mRNAs in the exponential growth phase in rich media.

***P. aeruginosa* proteins and their complexes.** Grad-seq primarily recover cytosolic proteins, as it is performed on a cleared lysate. Indeed, membrane-associated proteins were underrepresented among the ~2,200 detected proteins (Fig. 4A). For a quick overview of functional relationship of cosedimenting proteins, we clustered all detected proteins by principal-component analysis (PCA) according to their sedimentation profiles (Fig. 4B). Central regions in the plot correlate with sedimentation somewhere in fractions 4 to 10, i.e., complexes in the 200-kDa to 1-MDa range, clear examples of which are the clusters formed by RNAP or ATP synthase subunits. With respect to HMW fractions, ~6% of the detected proteins showed their main peak anywhere between fractions 8 and 20, where they are very unlikely to sediment on their own (Fig. 3A and 5A). In other words, most of these proteins were present in stable molecular complexes, indicating that they are associated with a protein or RNA partner to fulfil their function.

Next, we evaluated the integrity of complex sedimentation by manual inspection of established proteins, incorporating knowledge from other species such as *E. coli*. Many metabolic processes involve multienzyme complexes, some of which are giant. Several such large complexes can readily be discerned from our Grad-seq data (Fig. 5A), including all three dehydrogenase complexes: the pyruvate dehydrogenase complex (PDC), the oxoglutarate dehydrogenase complex, and the branched-chain α-keto acid dehydrogenase complex (Fig. 5B). Interestingly, all of these dehydrogenase multienzyme complexes sedimented as much smaller complexes than their suggested multimeric sizes. This observation is in agreement with a recently determined salt-labile structure of the PDC (38). The succinyl coenzyme A (succinyl-CoA)-synthetase $\alpha_2\beta_2$ complex, formed by the SucC and SucD proteins (39) from the TCA cycle, sedimented in fraction 3 (molecular weight [MW] of ~140 kDa). The aspartate carbamoyltransferase, which catalyzes the first step of the pyrimidine biosynthetic process, builds a complex of ~310 kDa and sedimented in fraction 5.

Examples of large complexes outside metabolic functions include the tetradecameric 840-kDa GroEL complex, here observed in fraction 7 (Fig. 5B). Interestingly, the functionally associated GroES complex sedimented away from it, in LMW fractions, as previously observed for *S. enterica* (22). A particularly large particle seems to be formed by the membrane-associated FtsH protease, which is a hexamer that goes on to form a 1-MDa holoenzyme with the membrane complex HflKC (40); we observed it in fraction 11. Importantly, we find dozens of additional proteins that sediment in HMW fractions (Fig. S2A). Since many of these are functionally uncharacterized, this region of the gradient bears great potential for discovery of new large protein complexes.

Topology of the *Pseudomonas* transcriptome. RNA-seq analysis of the gradient fractions revealed 4,643 transcripts above threshold (>100 reads in all fractions), covering 73.6% of the transcriptome (Fig. S1E). Quantitatively speaking, 84% of all reads came from rRNA (Fig. 6A). The class of tRNA contributed 6.5%, whereas reads from

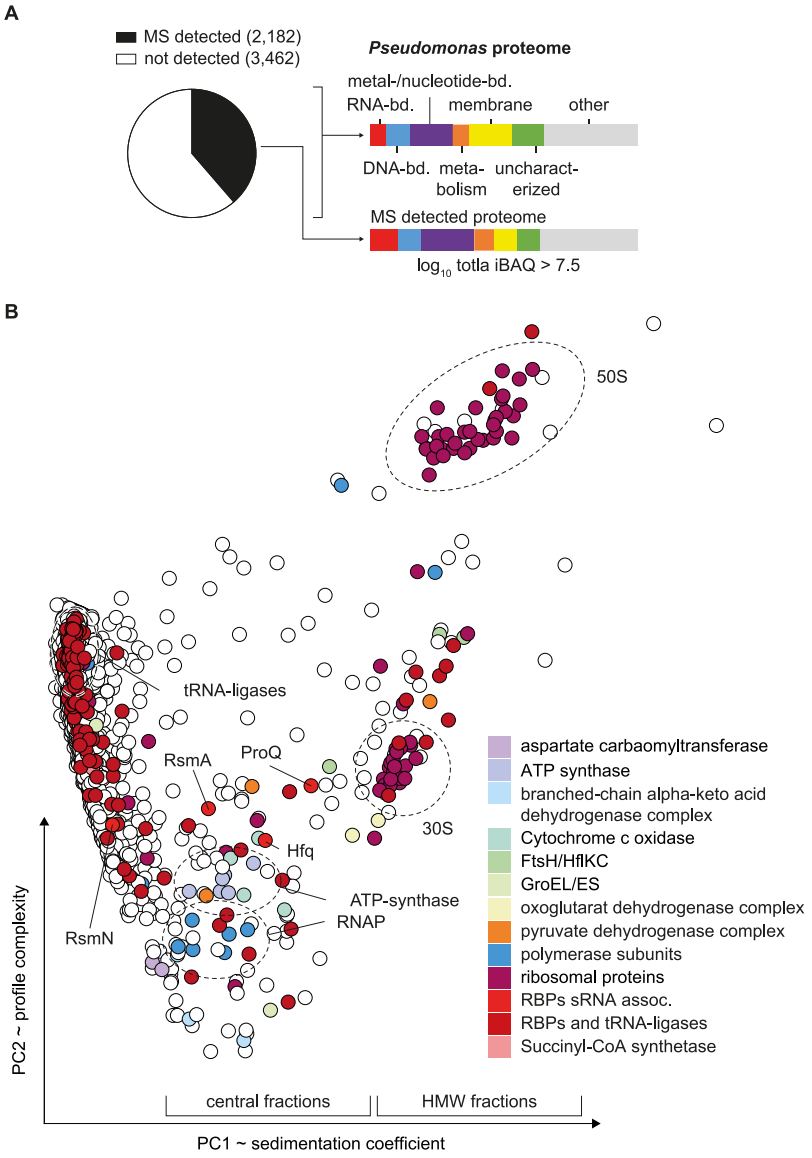

FIG 4 MS detection of complexes and RNPs. (A) A total of 2,182 proteins were recovered above the threshold of total iBAQ of >7.5 that represents approximately 40% of the total proteome. Membrane proteins (yellow) were depleted in the analyzed soluble fraction. (B) Twenty-one fraction sedimentation profiles were reduced in dimensionality to two principal components (PCs) resembling sedimentation complexity and coefficient. In the central part, RNAP and ATP-synthase complexes cluster in proximity with major RBPs Hfq, ProQ, and RsmA/N.

mRNAs were represented by ~9%. The diverse class of ncRNAs contributed 0.4% of all reads, i.e., markedly fewer than in previous Grad-seq of enteric bacteria in early stationary phase (for example, ~5% in *E. coli* [28]). Note that in *P. aeruginosa*, too, many ncRNA genes are only upregulated as the cells enter stationary phase (41).

For a better overview of the general sedimentation of all detected RNA classes, we reduced the complexity of the 21 fractions to six clusters (Fig. 6B). The mRNA reads were mainly found in fractions 3 to 8, coinciding with RNAP, and in the 30S subunit fractions 9 to 12 as well as in the pellet. This distribution differs from those of previous Grad-seq analyses of *E. coli*, *S. enterica*, and *S. pneumoniae* in which mRNAs generally cosedimented with ribosomes (22, 28, 29).

Systematic annotation of ncRNAs in *P. aeruginosa* lags behind that in other model gammaproteobacteria, with only 44 formally annotated ncRNAs (42) compared to

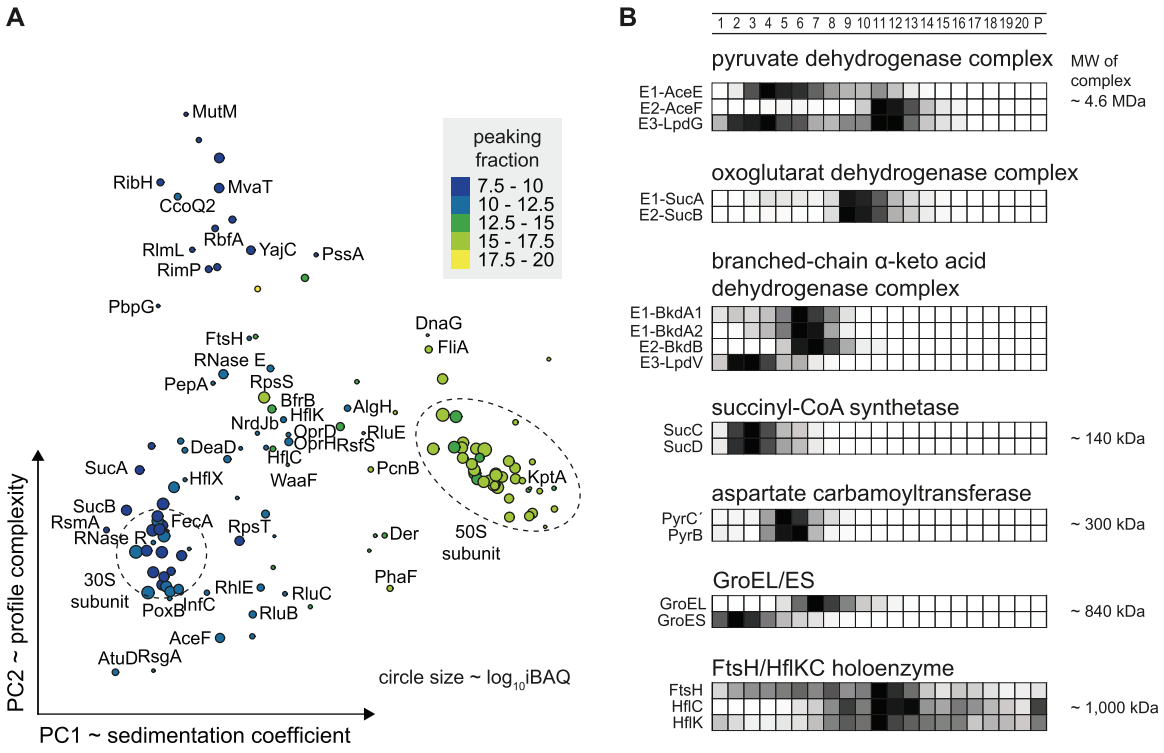

FIG 5 Large complexes cosediment in higher-molecular-weight fractions. (A) Sedimentation profiles of proteins that peaked in fractions 8 to 20 were clustered and labeled by protein name. Dashed circles indicate 30S and 50S ribosomal protein clusters. (B) Sedimentation profiles of metabolic complexes are listed with indicated calculated masses. The three dehydrogenase complexes sedimented between fractions 6 and 12. The TCA cycle complexes succinyl-CoA synthase and aspartate carbamoyltransferase sedimented in fractions 3 and 5, respectively. The chaperone GroEL sedimented in fraction 5, and the associated subunit GroES was dissociated and allocated to fraction 2. The protease complex FtsH/HflKC was detected in fraction 11. The relative abundance is ranging from 0 to 1 and is color coded in black.

hundreds each in *E. coli* and *Salmonella* and *Vibrio* species (43, 44). However, a total of 473 ncRNAs have been predicted in *P. aeruginosa* (45, 46), 336 of which were detectable in our Grad-seq data. Most of the *P. aeruginosa* ncRNAs and candidates thereof occurred in fractions 3 to 8, thus showing a general sedimentation profile similar to that of most mRNAs (Fig. 6B).

Stable noncoding RNA fragments overlapping with 5′ or 3′ untranslated regions (UTRs) constitute a potentially large class of bacterial riboregulators (47–50). Recent experimental transcriptome annotation (51–53) suggested that also in the *Pseudomonas* strain used here, many such UTR-derived candidate ncRNAs exist and accumulate to considerable levels. Here, we observe that such UTR fragments often showed a different sedimentation profile compared to that of the respective coding sequence (CDS) of the same mRNA (Fig. 6C). These include several UTR fragments that were recently observed to be highly enriched by coimmunoprecipitation with Hfq (8), which is a good indicator of potential cellular function as a base pairing small regulatory RNA (sRNA) (54). Obvious examples are the mRNA 5′ UTRs of phosphate transporter PA0450 and the uncharacterized proteins PA4643 and PA4972 or the mRNA 3′ UTRs of putative transcriptional regulator PA2758, cyclic guanylate-specific phosphodiesterase PA3825, and serine dehydratase SdaB, all of which peak at least four fractions away from the CDS part of their parental mRNAs (Fig. 6C). With respect to the published literature, RhlS is an activating 5′ UTR-derived ncRNA from the *rhlI* gene (55). While the precise mechanism whereby RhlS promotes expression of the *rhlI* mRNA is currently unknown, we notice that the two RNAs occur in different fractions (Fig. 6C), supporting the proposed model of an independent regulatory function of the 5′ UTR.

To validate the Grad-seq-based detection of UTR-derived fragments, we chose to

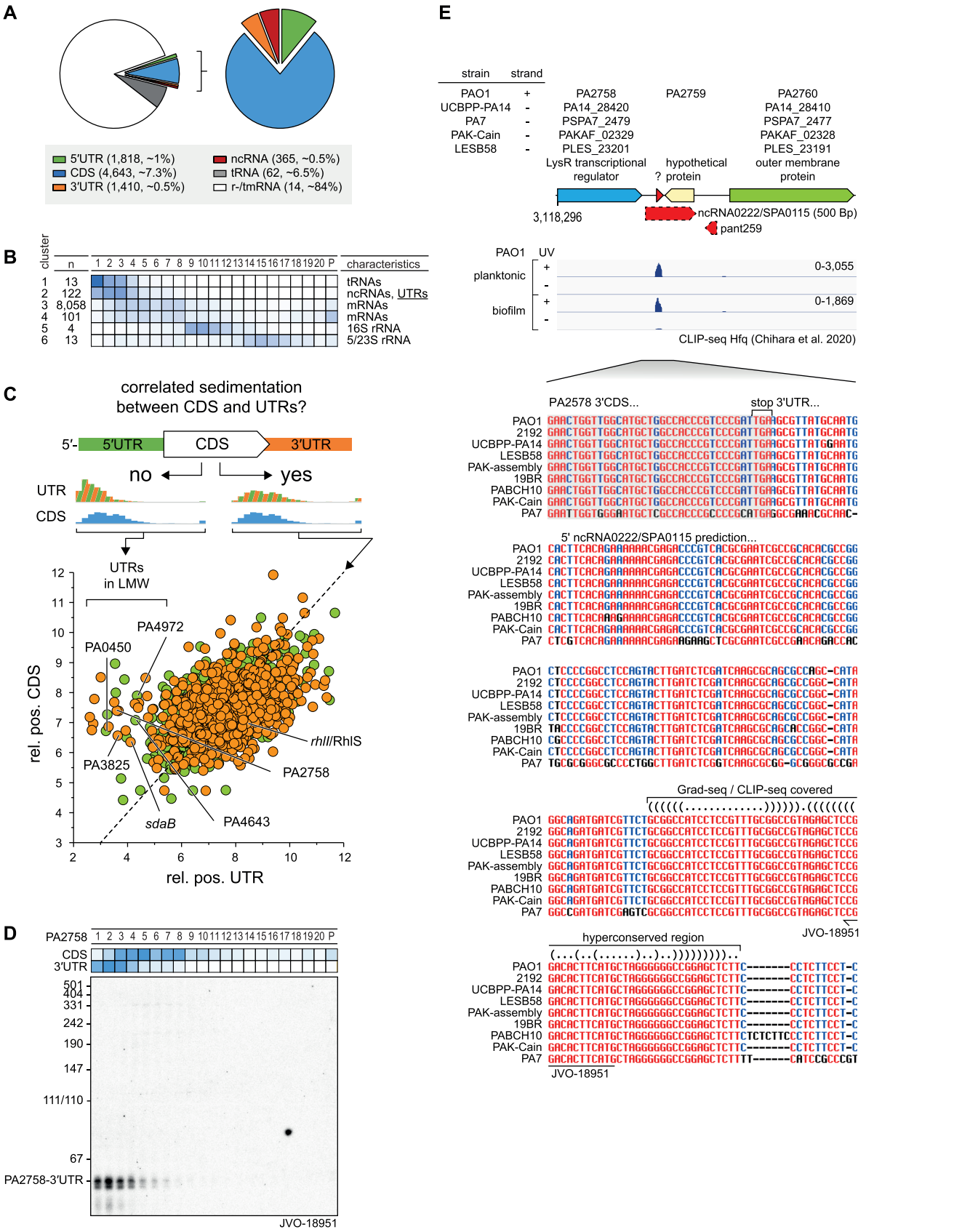

FIG 6 Sedimentation of RNAs. (A) In total, 73.6% of the *P. aeruginosa* PAO1 transcriptome was detected. mRNAs represented approximately 9% and ncRNAs approximately 0.4% of sequenced reads. (B) RNAs were clustered based on sedimentation position.

(Continued on next page)

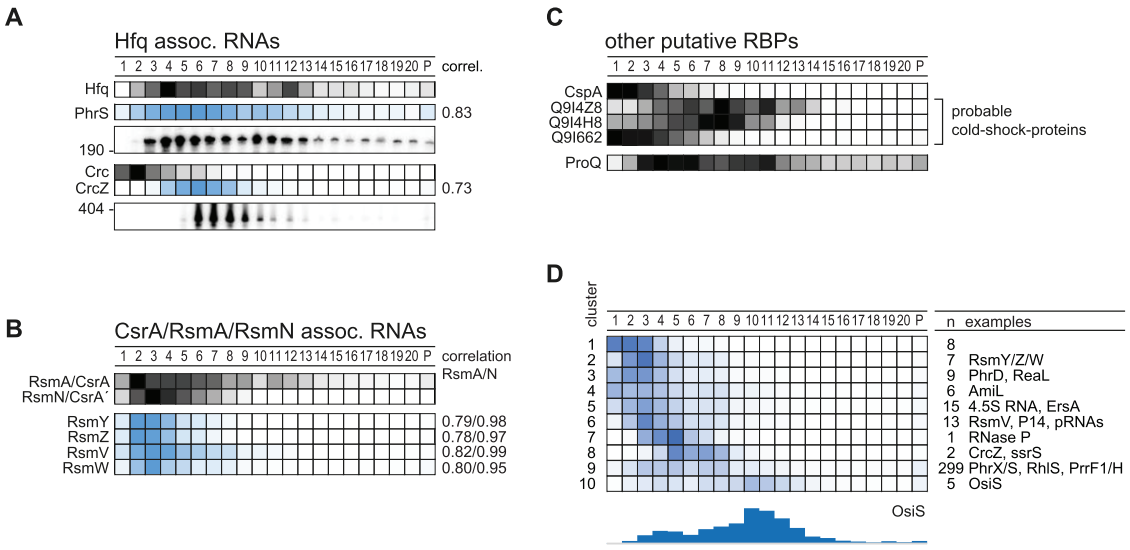

FIG 7 RBPs cosedimented with targeted RNAs. (A) Hfq-associated RNAs cosedimented in a correlated fashion (>0.7) with Hfq mainly in fractions 3 to 8. (B) The same holds true for Rsm RNAs and the corresponding RBPs RsmA and RsmN. (C) Other putative RBPs are the cold shock protein CspA and three putative Csps that sedimented in the first fractions as also previously reported. The FinO-domain protein ProQ sedimented, interestingly, in between fractions 4 and 11. (D) Clustering of annotated ncRNAs by sedimentation position revealed clusters that could be bound by novel RBPs. Interestingly, 5 ncRNAs sedimented in 30S subunit fractions, e.g., OsiS.

probe the 3′ UTR of PA2758 mRNA on a Northern blot. We readily detected a distinct ~50-nt RNA species with the predicted sedimentation in fractions 1 to 4, distinct from the full-length PA2758 mRNA (Fig. 6D). This 3′ UTR RNA species was much shorter than the previously predicted ncRNA candidate ncRNA0222/SPA0115 from this genomic region (46). Importantly, however, it comprises the most conserved part of the 3′ UTR in question, which includes the predicted Rho-independent transcriptional terminator of PA2758 (Fig. 6E). In addition, this ~50-nt RNA species was recently shown to be highly enriched in global Hfq coimmunoprecipitation experiments (8) (Fig. 6E), indicating that it might function as a base-pairing sRNA.

In silico target prediction using the CopraRNA algorithm (56) supports the notion that the 3′ UTR of PA2758 might act in *trans* to regulate mRNAs by base pairing (see Fig. S3). Focusing on potential binding sites around the start codon of mRNAs, CopraRNA predicts as the top target an extended interaction that might translationally inhibit the mRNA of *napC*, which is the last gene in the *napEFDABC* operon encoding nitrate reductase. Importantly, base pairing would crucially engage a 13-nt-long single-stranded region of the PA2758 3′ UTR, which looks like a conserved seed sequence of this sRNA. Further studies are required to validate this particular prediction and to determine the targets of the UTR-derived sRNAs proposed here.

Major RNA-binding proteins and associated ncRNAs. *P. aeruginosa* is known to possess two large posttranscriptional networks that depend on globally acting RBPs: one governed by Hfq and the other by two CsrA-like Rsm proteins. The mRNA and ncRNA ligands of these RBPs have been mapped in a transcriptome-wide fashion (8, 9, 17, 19), albeit not in the growth phase studied here.

The 190-nt PhrS ncRNA, known as a direct activator of the mRNA of the transcriptional regulator PqsR (57), is a well-characterized target of Hfq. PhrS is readily detected

FIG 6 Legend (Continued)
ncRNAs accumulated together with UTRs in cluster 2. (C) Comparison of relative positions of CDS and corresponding UTRs revealed differential sedimentation that attributed to processing and rise of ncRNAs fragments. (D) The 3′ UTR region of PA2758 was probed by Northern for a 50-nt fragment, position was determined previously based on read-coverage in the annotated UTR. (E) An alignment of the 3′ UTR region of PA2758 revealed a conserved motif in the read-covered part (red arrow). RNA Co-fold (https://e-rna.org/cofold/) resembled a two-stemmed structure that is indicated in the dot-bracket annotation.

in the gradient by both RNA-seq and Northern blot and shows a very similar sedimentation profile to that for Hfq (Fig. 7A). Its absence from fractions 1 and 2 suggests that this ncRNA is always present in complex with Hfq and/or other interactors.

Another well-characterized Hfq-related ncRNA is CrcZ. This ~400-nt ncRNA forms a stable complex with Hfq and Crc (12), which prevents the Hfq/Crc complex from repressing translation of *amiE* mRNA (58). The CrcZ RNA sediments in fractions 6 to 9 (Fig. 7A), in which Hfq is also found. Indeed, the in-gradient profiles of both the PhrS and CrcZ ncRNAs are well correlated with that of Hfq (coefficient, >0.7), suggesting a stable molecular interaction (Fig. 7A). In contrast, the Crc protein peaks far away, in LMW fraction 2, suggesting that the Hfq/Crc/RNA complex is unlikely to exist under the rich medium conditions used here (as predicted previously [13]). Additional explanations include that the Hfq/Crc targets are rapidly degraded, leading to disassembly of the Hfq/Crc/mRNA complexes, or that these complexes are simply too labile in a glycerol gradient.

Regarding the Rsm network, the RsmA protein alone is known to regulate—directly or indirectly—9% of the transcriptome (7, 19, 59). RsmA blocks translation by binding to GGA motifs in mRNAs; its own activity is also regulated at the RNA level, by the ncRNAs RsmY/Z/V/W, which sponge RsmA by presenting multiple GGA motifs (60). The homologous RBP RsmN acts and is acted upon in the same fashion (15, 17, 18). Here, we observe well-correlated sedimentation of the two Rsm proteins and its four-known decoy RNAs, suggesting that in exponentially growing *Pseudomonas* cells (Fig. 7B), these two RBPs are largely kept inactive by their ncRNA antagonists. The more abundant RsmA also sedimented in ribosomal fractions, perhaps in association with polycistronic mRNAs. In any case, the RsmA/N profiles are clearly distinct from those of Hfq and its associated RNAs.

Other RBPs and candidates thereof with unknown ligands also show intriguing sedimentation profiles. Proteomics detected the cold shock-like protein CspA in the first fractions (Fig. 7C), which is in agreement with Grad-seq profiles of CspA in *E. coli* and *Salmonella* (22, 28). Cold shock proteins, while interacting with many cellular transcripts, bind their targets with low affinity (26), which may explain their accumulation in LMW fractions. Intriguingly, while one of the three other CspA-like proteins of *P. aeruginosa* shows a congruent sedimentation profile, the other two migrate toward the middle of the gradient. Thus, these two putative RBPs, PA0961 and PA1159, represent strong candidates for cold shock proteins that engage in stable complexes with either RNA or other proteins (Fig. 7C).

Chromosomally encoded RBPs with a FinO domain such as ProQ have recently emerged as the third major ncRNA-associated RBP in enteric bacteria (25). Based on a Pfam prediction (61), we propose protein Q9I0Q4 as the putative ProQ homolog in *P. aeruginosa*. Peptides of it can be detected in almost all gradient fractions, although the majority of them are found in fractions 3 to 11 (Fig. 7C). This ProQ profile is broader than in *E. coli* or *Salmonella*, especially with respect to *P. aeruginosa* ProQ appearing in 30S ribosome fractions. In any case, this broad sedimentation argues for *P. aeruginosa* to possess functional FinO/ProQ-like RBPs.

To obtain a focused overview of ncRNA sedimentation patterns for potential cross-comparison with RBPs, we clustered all 365 detected and candidate ncRNAs according to their sedimentation profile, yielding 10 clusters (Fig. 7D). Approximately three-quarters of these ncRNAs end up in cluster 9, which includes the well-characterized Hfq-associated ncRNA PhrS and PrrF1 (57, 62) and PhrX (63). In essence, many of these ncRNAs sediment like mRNAs (Fig. 6B, cluster 4). This is particularly pronounced with the five members of cluster 10, challenging the previous annotation of these transcripts as noncoding RNAs. For example, OsiS (PA0611.1, pant67 [45]) has been suggested to act as a regulatory RNA to link oxygen level sensing to the production of quorum sensing molecules (64). However, the comigration of these transcripts with 30S ribosomes suggests the possibility that they possess overlooked small ORFs. Note that a putative 30S association recently guided the discovery of a functional small ORF

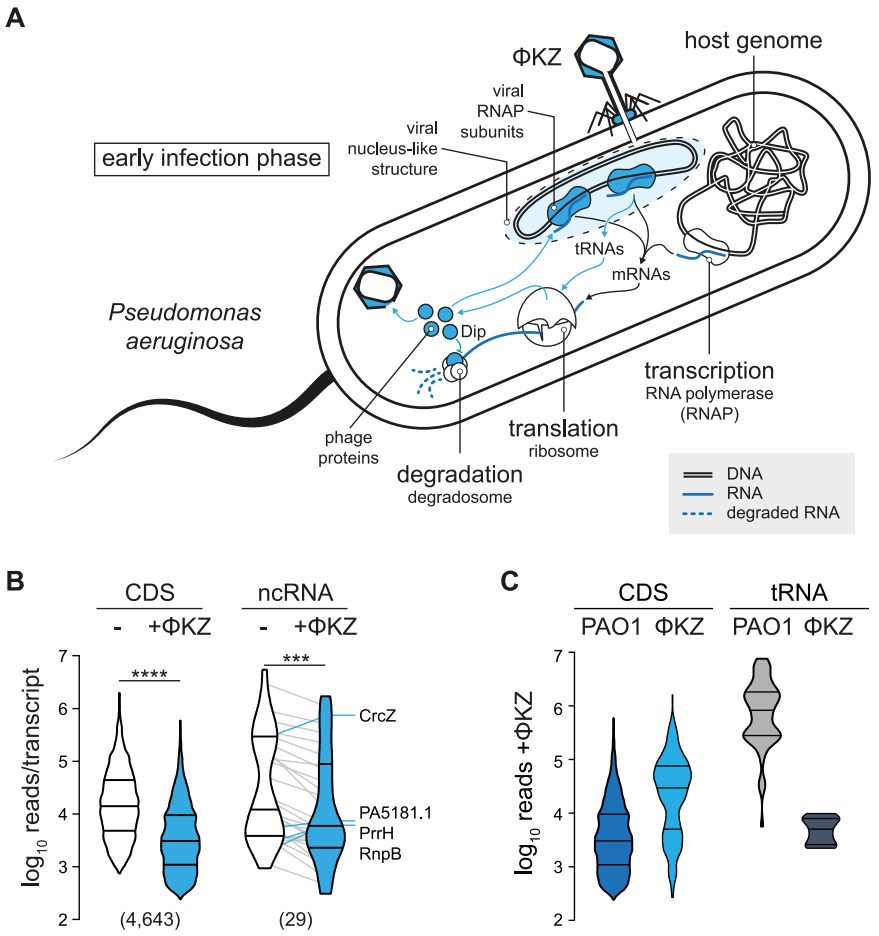

FIG 8 Host RNome is altered at early infection. (A) ΦKZ conquering of *Pseudomonas* is strongly linked to modulation of RNA homeostasis. Viral RNAPs are utilized and produced to transcribe phase genes. Additional phage tRNAs are utilized in translation, and the RNA degradation is blocked through the Dip protein. (B) Host CDS and ncRNA levels were significantly reduced by approximately 5-fold in a nonparametric paired *t* test. The threshold for statistical significance was a two-tailed *P* value of <0.05. ***, $P < 0.001$; ****, $P < 0.0001$. Prism 9 was used for statistical analyses. Lines connect individual RNA levels. Outliers that increased levels upon ΦKZ infection are labeled. (C) Individual phage CDS are two magnitudes more abundant than host RNAs, whereas phage tRNAs remain underrepresented 10 min postinfection.

in the seemingly noncoding RyeG RNA of *E. coli* (28, 65). In the present case, recent *P. aeruginosa* ribosome profiling (Ribo-seq) data (66) provide additional support for our prediction that OsiS is translated into a protein (see Fig. S4).

Phage-induced stress affects cellular organization of the RNome. The in-gradient distributions of RNA and protein described above reflect the complexome of *P. aeruginosa* under optimal growth conditions, characterized by a rich supply of nutrients and rapid growth. To determine how this molecular organization is perturbed by a biotic stress, we subjected *P. aeruginosa* to infection by a phage, specifically, the lytic giant phage ΦKZ, which is a well-established model phage of pseudomonads and known to usurp many cellular functions of its host (67–69) (Fig. 8A).

Performing Grad-seq on *P. aeruginosa* cells after 10 min of infection by phage ΦKZ, we found that phage transcripts accounted for ~3% of all reads, while the host mRNAs remained at ~7% (see Fig. S5). Nonetheless, a paired *t* test showed that the sum of all host CDSs and ncRNAs at this early infection time point was approximately 5-fold lower than in uninfected cells, notwithstanding a few prominent outliers such as the ncRNAs CrcZ, PrrH, and RnpB (Fig. 8B). At the same time, the individual ΦKZ transcript exceeded the typical host transcript in abundance by 1 order of magnitude (Fig. 8C).

While altered abundance of host transcripts is one consequence of phage predation, we were particularly interested in the possibility that the phage infection might also perturb host transcriptome organization, altering the association of host transcripts with cellular factors to promote viral replication. Such changes, which should be visible as shifts in the gradient, could point out stress response mechanisms and pathways that remain invisible in standard RNA-seq experiments.

Focusing on transcripts with a <3-fold change in total level, we indeed observed hundreds of transcripts with negative or positive shifts in their sedimentation profile (Fig. 9A and B). An excellent example is given by the mRNAs of the uncharacterized proteins PA4441 and PA2746a, which both showed redistribution toward fractions 10 and 11, possibly reflecting increased translational initiation by 30S ribosomes. Another example is *liuR*, coding for the transcriptional regulator of the of metabolic *liu* genes (70) (Fig. 9A and C). Similarly, we predict several host ncRNAs to reassociate with different partners in the early phase of phage infection, illustrative examples of which are ErsA, pant512, and pant253 (Fig. 9D). In contrast, with the exception of $tRNA^{Leu}$, transfer RNAs generally stayed in the same fraction after ΦKZ infection (Fig. 9A to C).

ErsA is a well-characterized small RNA of *P. aeruginosa* which has been proposed to serve a dual regulatory role in biofilm development, activating the mRNA of transcriptional regulator AmrZ while at the same time repressing the mRNA of AlgC, an important virulence-associated enzyme for the production of sugar precursors (71, 72). In addition, ErsA acts as a translational repressor of the mRNA of outer membrane porin OprD (73). ErsA is well expressed during the exponential growth phase (51) and bound by Hfq (8), making it an excellent candidate for validation by an independent technique of the infection-dependent changes seen in Grad-seq. Using an oligonucleotide probe for ErsA, we probed all 20 gradient fractions plus the pellet by Northern blotting. Intriguingly, this method showed even more clearly that ErsA, 10 min into phage infection, is depleted in LMW fractions, with its main peak shifting to fractions 10 and 11 where 30S ribosomes sediment (Fig. 9E). A similar albeit less pronounced shift was observed for the PhrS ncRNA. In contrast, phage infection did not affect the in-gradient distribution of 5S rRNA and 6S RNA, as predicted by the digital data. While the biological meaning of the redistribution of ErsA remains to be understood, its independent validation by Northern blotting adds confidence for the predicted infection-induced shifts of other cellular transcripts.

Phage mRNAs are efficiently transferred from transcription to translation. At the early time point of ΦKZ infection used here, nearly all (366/376) annotated phage genes (NCBI nucleotide accession NC_004629.1) are expressed (Table S1) (30, 51). For an initial glimpse at the sedimentation profiles of phage transcripts, we probed two well-expressed viral operons on Northern blots; specifically, operons 54 and 88 (30), which encode metabolic and structural proteins of the phage, respectively. Intriguingly, in both cases, the strongest signals obtained were from the pellet fraction, indicating that these mRNAs are heavily engaged by the translation apparatus (Fig. 10 and Fig. S5F and G). In addition, signals within the gradient were primarily seen in fractions 10 to 13, overlapping with the 30S ribosome peak.

Global inspection of the Grad-seq data reinforced the notion that phage mRNAs are prioritized for translation. That is, in contrast with host mRNAs which were primarily detected in fractions 3 to 8 (Fig. 6B), the phage mRNAs were clearly more abundant in fractions containing 30S and 70S ribosomes (Fig. 10B and C). In addition, different from host tRNAs, the phage-encoded tRNAs also appeared in the 30S-containing fractions (Fig. 6B and 10C; Fig. S5E and F), which appears to be a type of association (74). Thus, two classes of ΦKZ transcripts indicate the existence of mechanisms that ensure efficient synthesis of phage proteins.

Grad-seq guides the identification of phage-encoded ncRNAs. We reasoned that if phage mRNAs generally comigrate with ribosomes, noncoding phage transcripts might be revealed through different in-gradient distributions, as already evident from the phage-encoded tRNAs. Indeed, manual inspection of Grad-seq profiles along the 280-kbp phage genome revealed two ncRNA candidates. The first example was an

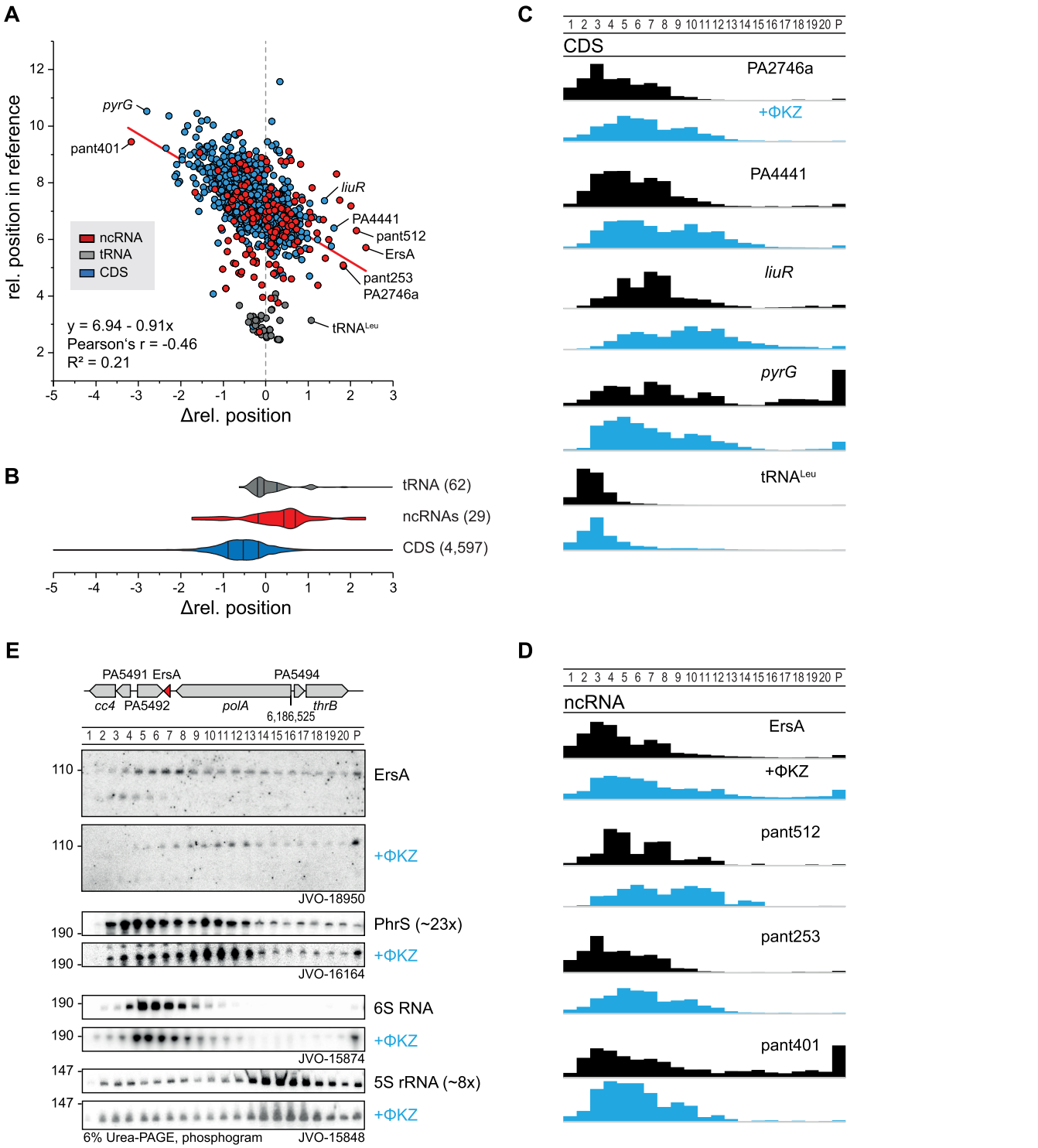

FIG 9 ΦKZ infection shifts transcripts and ncRNAs. (A) Transcripts that sediment in HMW fractions are more shifted toward LMW fractions (change in level, <3-fold). (B) Annotated ncRNAs were shifted in direction of HMW fractions. (C) Sedimentation profiles of host CDS that shift strongly toward H/LMW fractions from panel A. (D) Sedimentation profiles of phage-infection affected host ncRNAs, of which, ErsA represents an important regulator in biofilm formation and is shifted to HMW fractions. (E) The ErsA shift in sedimentation was validated by Northern probing against the end of stem-loop I in ErsA and accumulated strongly in the pellet fraction. A less pronounced shift was observed for PhrS that was strongly depleted upon infection.

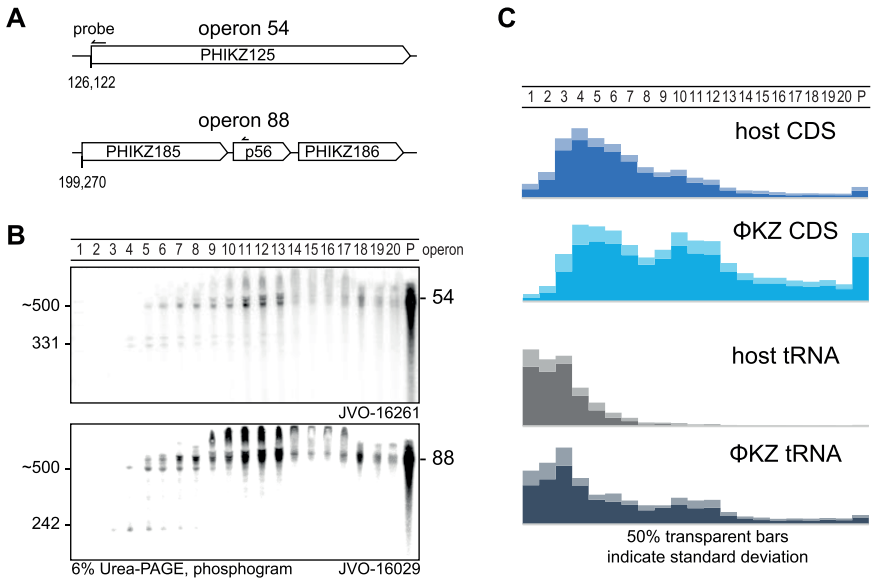

FIG 10 Phage RNAs associate strongly with ribosomes. (A and B) Expression and sedimentation of early infection operons 54 and 88 was Northern probed and revealed a strongly ribosome-associated profile. Interestingly, smaller fragments sedimented exclusively before fraction six. (C) In general, phage transcripts sedimented substantially at ribosomal fractions, indicating an efficient transfer to translation or stabilization at the ribosome. Phage tRNAs were also strongly utilized in translation or stabilized at ribosomal subunits, judged by sedimentation in ribosomal fractions.

~100-nt RNA species from the intergenic space between phage genes PHIKZ298 and PHIKZ297, predicted to sediment primarily in fractions 3 and 4 (Fig. 11A and B). Northern blot probing proved this species to be abundant and also confirmed its predicted length. Interestingly, the probe used here simultaneously detects a larger transcript(s) with an mRNA-like in-gradient distribution. Combined with the lack of a mapped transcription start site (TSS) downstream of the stop codon of PHIKZ298 (51), we assume that the detected 100-nt RNA species is generated by 3′ UTR processing of the PHIKZ298 mRNA. According to *in silico* prediction, the ncRNA forms two stem-loops, the second of which might constitute the Rho-independent transcriptional terminator of the PHIKZ298 gene (Fig. 11C).

The other ncRNA candidate also accumulates in the LMW part of the gradient yet shows a broader distribution (fractions 4 to 10) (Fig. 11A and D). This putative ncRNA comprises the first 180 nt of the 5′ UTR of phage gene p40. Similar to the above-described candidate, Northern blot probing both confirmed the proposed length of the candidate ncRNA itself and detected larger transcripts with mRNA-like behavior in heavier fractions. Note that for reasons unknown, the signals of both these putative ncRNAs are shifted by one fraction toward the top of the gradient when comparing the Northern blot to the Grad-seq data. The 5′ UTR-derived ncRNA species also seems highly structured, showing two stem-loops (Fig. 11E), the second of which might promote premature termination before transcription reaches the start codon of p40.

We carefully checked both UTR-derived RNA species for potential small ORFs, including alternative start codons, but found none that would be preceded by a strong Shine-Dalgarno sequence. We therefore consider both as ncRNAs and take them as illustrative examples how the extra information provided by Grad-seq, compared to that by simple RNA-seq, may help to discover overlooked transcripts in phage genomes.

DISCUSSION

The primary objectives of this work have been (i) to provide the interested microbiologist with previously unavailable Grad-seq profiles of cellular transcripts and proteins in the model bacterium *P. aeruginosa* from a commonly studied growth condition, (ii)

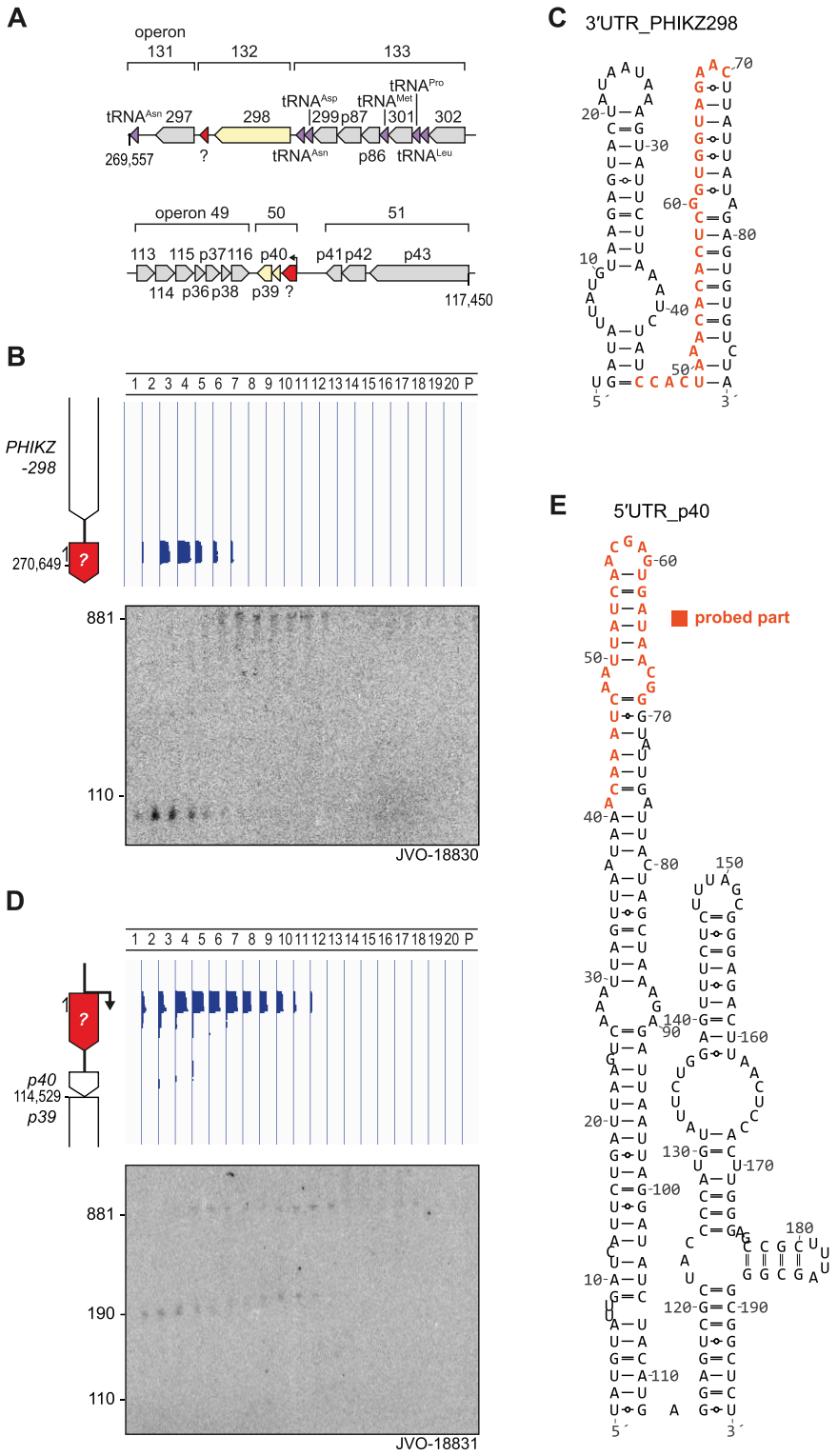

FIG 11 Grad-seq guides the discovery of phage-related ncRNA candidates. (A) Loci of operons 132 and 50 including candidate ncRNAs. (B) In the 3′ UTR of PHIKZ298, we observed sedimentation exclusively around fraction four that was confirmed by probing an ~100-nt fragment that M-folded (109) into a two-stemmed structure (C). (D) Read-coverage profiles in the 5′ UTR of p40 revealed an LMW-weighted sedimentation profile different from that of phage CDS transcripts (Fig. 10C). An ~180-nt fragment was detected in RNAP-associated fractions and at 30S subunit fractions. A longer fragment (~880 nt) was substantially shifted to fraction 12. (E) The 5′ UTR-p40 fragment M-folded into a two-stemmed structure. Northern probing was conducted against the nucleotides indicated in orange.

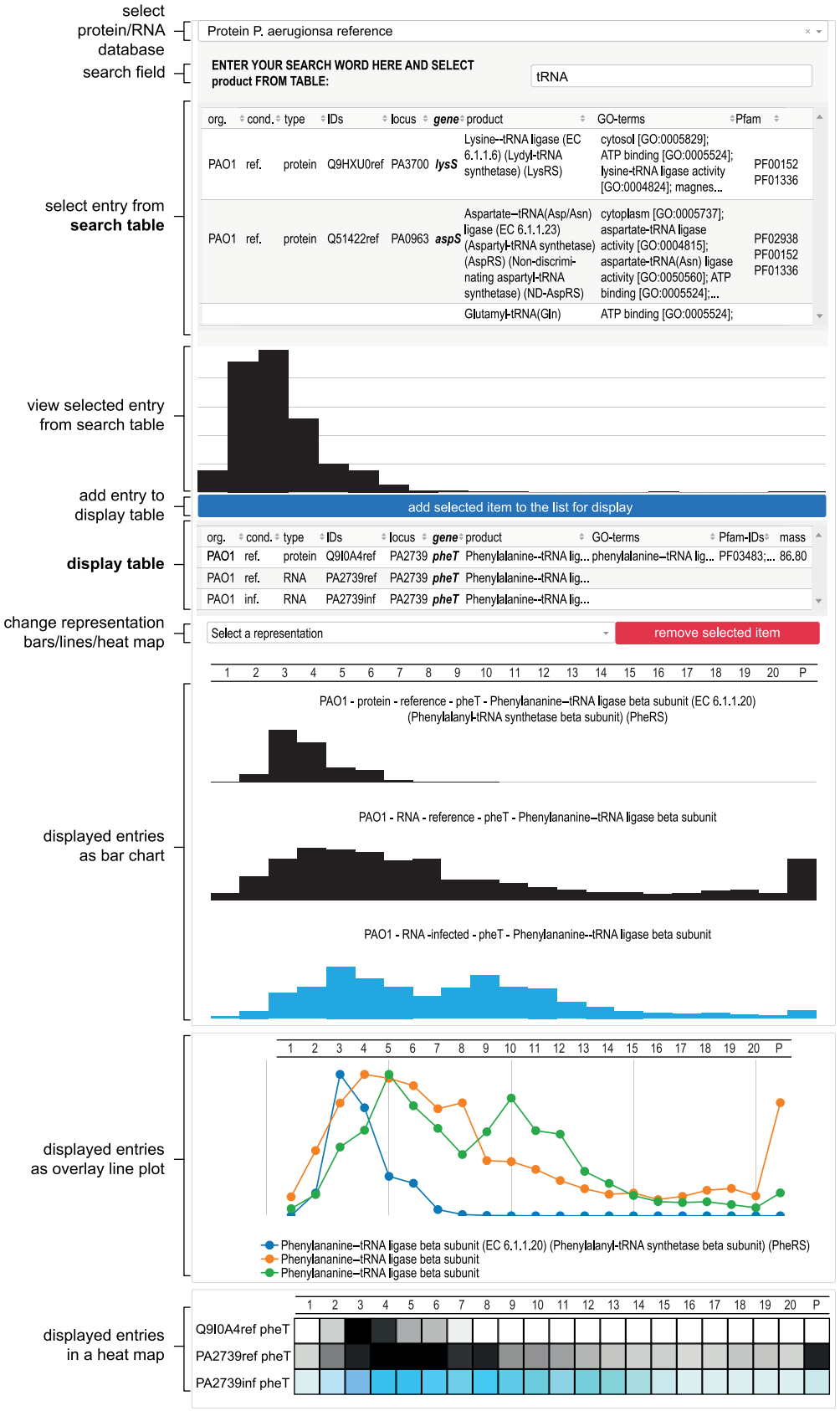

FIG 12 Differential Grad-seq browser. Protein and RNA sedimentation profiles can be searched for noninfected and infected experiments. Selected entries are displayed as a bar chart and can be added in a display list that is plotted as bar chart, lines, or heat map. The browser is accessible at https://helmholtz-hiri.de/en/datasets/gradseqpao1/.

to assess the quality of these high-throughput results by independent methods, (iii) to illustrate how the technique might be utilized in the future to study bacteriophage-host interactions, and (iv) to organize the data such that they can be accessed and interrogated by nonspecialists. To facilitate the latter, we have set up an online browser (Fig. 12), which is available at https://helmholtz-hiri.de/en/datasets/gradseqpao1/ and allows the user to cross-compare the present *Pseudomonas* data with Grad-seq results for several other species (22, 28, 29). In addition, the browser offers comparison with GradR (75), which is a recently developed variation of Grad-seq trying to predict potential RNA association/dependency of cellular proteins and, more specifically, unrecognized RBPs. Although those GradR data were obtained with *Salmonella*, some of the many proteins affected by the RNase treatment used in this method will also be conserved in *P. aeruginosa*.

Even though the present *P. aeruginosa* Grad-seq data cover only one growth condition, we believe that they already offer a huge discovery space. Given the bacterium's impressive metabolic capabilities, the mass spectrometry (MS) profiles of all detected proteins should give new insights into metabolic multienzyme complexes. Obviously, not all these complexes are sufficiently stable to survive the long (overnight) ultracentrifugation procedure during which cellular complexes separate according to size and shape in a glycerol gradient. For example, the PDH complex dissociated into stable smaller subcomplexes (Fig. 5B), which is in keeping with recent size exclusion experiments that revealed a salt-labile structure of the macromolecular complex (38). Nonetheless, in addition to the examples highlighted in Fig. 5B, there are many proteins that sedimented between the fractions of the small and large ribosomal subunits. In other words, these proteins must be part of stable complexes in the 2- to 4-MDa range, information that should provide useful leads for future functional analysis.

From an RNA biology perspective, the initial Grad-seq data provided here promise to be a treasure trove. Known RBPs such as Hfq and RsmA/N sedimented in a much higher molecular weight range than their individual size would predict. We have recently shown for Hfq (and other RBPs) in *Salmonella* that this sedimentation behavior is primarily due to RNA interactions. Indeed, when transcripts are removed by RNase treatment of the lysate, these proteins shift to LMW fractions (75). In the present *P. aeruginosa* data, the associations of the Hfq and RsmA/N RBPs are also obvious by a clear comigration with their major RNA ligands (Fig. 7A and B). While these three RBPs have seen extensive work, our Grad-seq data strongly indicate that there is yet another global RBP. That is, we have detected peptides of a candidate ProQ RBP (protein PA2582), which is encoded in a chromosomal region close to exonuclease repair gene *uvrC* and the regulatory protein PA2583 (see Fig. S6 in the supplemental material). The predicted ProQ of *P. aeruginosa* not only carries a full-length FinO domain, it also shows conservation of several important residues for RNA binding by *E. coli* ProQ (76). The pseudomonal ProQ proteins are small (~20 kDa) and, similarly to *Neisseria* ProQ (21), lack the typical C-terminal or N-terminal extensions of the central FinO domain (25), which makes them attractive candidates for understanding the core recognition mode of RNA by the FinO domain.

The complex of 6S RNA and RNAP is an RNA-based regulation previously undescribed in *P. aeruginosa*. The two partners show in an almost ideal form both narrow peaks and exceptionally high correlation in the gradient, primarily in fractions 5 and 6 (Fig. 2A). While similarly high correlations have been shown before in both conventional and Grad-seq-based analyses of 6S RNA-RNAP (22, 28, 29), the new observation in the present *P. aeruginosa* Grad-seq experiment are the 14-nt pRNAs. These pRNAs are a natural product of the 6S RNA regulatory cycle in which 6S RNA captures RNAP by mimicking an open promoter complex of transcribed DNA and, once bound, changes the affinity of RNAP for different σ factors, the result of which is a global change in transcription (34). In order to dissociate from 6S RNA, RNAP uses it as a template for transcription, yielding pRNAs. Thus far, these pRNAs have been considered an inevitable side product of 6S RNA release, possessing no independent function and awaiting degradation. However, our detection of a pRNA peak spanning several

fractions (2 to 5) may now hint that these short transcripts go on to interact with other cellular molecules, perhaps to serve a currently unrecognized independent function in the cell.

Next to Grad-seq analysis of naive *P. aeruginosa* cells, we provide an RNA snapshot with the corresponding experiment performed at an early time point of phage infection. Phages by definition manipulate host cell metabolism in exquisitely diverse ways, as reviewed recently (68). Specifically, *Pseudomonas* bacteriophage ΦKZ is known to rapidly shift toward host-independent viral replication. This is achieved through transcription by both virion-delivered and virus-encoded RNAPs (30), a complete reorganization of the metabolism (77), and modulation of the host RNA turnover machinery (78). However, insights into RNA/protein interactions between phage and host remain scarce. Therefore, the RNA data provided in the next section allow a first glimpse at how ΦKZ alters RNA processing in the host and hint at modulation of translation rates of some host mRNAs, and of phage mRNAs, in general. Importantly, active manipulation of protein synthesis has been reported for coliphages T4 (79) and T7 (80–84) and is also implied by prediction of phage-encoded S1 proteins (85, 86).

On the host side, phage infection impacts the in-gradient distributions of both mRNAs and ncRNAs. Many host mRNAs shift away from ribosomal fractions, and this effect is even more pronounced for those transcripts with a particularly strong ribosome association in the first place. Primary examples include transcripts related to oxidative phosphorylation (see Fig. S7); a strong reduction of the synthesis of these proteins may eventually lead to a collapse of cellular energy production. In general, given that active translation stabilizes bacterial mRNAs, the predicted interruption of translation may offer one explanation for the observed ~5-fold depletion of host transcripts 10 min after phage infection.

Yet, we also observe the reciprocal behavior, i.e., host mRNAs that move into ribosome-associated fractions. A particularly noteworthy case is the mRNA of protein PA4441, which carries a predicted DUF1043 domain that is also found in cyclic oligonucleotide-based anti-phage signaling system (CBASS) effectors (87). Put simply, after phage predation, the mRNA of a potential phage defense protein migrates to the 30S-related fraction as the consequence of increased translational initiation. This may indicate the existence of a specific mechanism to rapidly activate synthesis of host proteins with protective functions.

In addition to mRNAs moving out of or into ribosomal fractions, Grad-seq predicts interesting cases of ncRNAs that seem to associate with different or additional cellular partners after lytic infection. These shifts for the ErsA and PhrS sRNAs were independently validated on Northern blots (Fig. 9E). Because both of these ncRNAs are well characterized, they would serve as ideal models to understand the mechanisms behind the observed shift. In the case of PhrS, it is worth mentioning that in *P. aeruginosa* strain PA14, this sRNA may promote adaptive immunity against bacteriophages through suppression of Rho-dependent termination of early CRISPR transcripts (88). This CRISPR leader is conserved in the PAO1 strain used here despite the lack of a CRISPR array, and we thus speculate that the observed shift of PhrS RNA might be the result of enhanced PhrS-CRISPR leader interaction upon phage infection.

Of well-understood molecular mechanisms whereby phages usurp bacteria, several include active manipulation of host RNA decay (89, 90). The present Grad-seq data are of insufficient depth to allow for a statistically sound global analysis of phage-induced alteration of host RNA processing. However, during inspection of rRNA profiles, we observed that biogenesis of 5S rRNA in phage-infected cells might be compromised, as suggested by a smeary Northern blot signal for 5S rRNA in several gradient fractions (see Fig. S8A). Processing of 5S rRNA from longer ribosomal transcripts crucially depends on the major endoribonuclease RNase E, and ΦKZ expresses a protein called Dip that functionally interferes with the RNase E-associated degradosome (78, 89, 91).

In further support of altered RNase E activity, we observe a differential accumulation of 5′ mRNA fragments of RNase E itself (Fig. S8B and C), which is well established to

cleave in the 5′ UTR of its own mRNA to feedback-control its own protein levels (92–94). Upon ΦKZ infection, a longer band that we attribute to cleavage at the *rne-II* motif (Rfam RF01756 [95]) disappears. Whether the altered processing eventually causes a decrease in RNase E protein levels needs to be shown. Interestingly, this mechanism would be the opposite to what was reported with the marine cyanobacterium *Prochlorococcus* MED4, in which phage infection boosts RNase E synthesis by altered processing of its mRNA (96).

Finally, one of the most intriguing phage-related observation in our Grad-seq data is the distribution of phage versus host mRNAs. Contrary to mRNAs for which reads where detected in both LMW and ribosome-containing HMW fractions (Fig. 3B and S5E), phage mRNAs sedimented almost exclusively in the HMW part of the gradient as well as in the pellet (Fig. 10C and S5F and G), the latter of which contains 70S monosomes and polysomes. This would suggest that ΦKZ mRNAs are prioritized for translation, perhaps even at the expense of making host proteins, as has been reported previously in other systems (79–86) We would like to caution, however, that mRNA reads in LMW fractions represent a steady-state picture in which we see host mRNAs undergoing degradation, whereas the newly produced phage mRNAs, only 10 min after the phage has attacked, may still be fully protected by ongoing translation. In addition, phage ΦKZ segregates its DNA from immunity nucleases of *P. aeruginosa* by constructing a proteinaceous nucleus-like compartment (69), which might provide further protection of phage mRNAs. While this new model does not question generally that phage mRNAs are translated by cytoplasmic ribosomes, the influence of this intracellular spatial segregation on phage mRNA stability is not clear. Future work with higher time resolution will be needed to determine whether phage mRNAs are indeed prioritized for translation and, if so, which phage or host factors are responsible.

Many of the above-described observations will benefit from a further mechanistic analysis of the Grad-seq protein data of infected host cells, which is currently ongoing. In studying the molecular mechanisms governing phage-bacteria interactions, it should be obvious that Grad-seq offers unique opportunities to reveal RNA-protein interactions, including phage-CRISPR-Cas complex interactions, usage and modifications of tRNAs, or the discovery and functional elucidation of phage ncRNAs, all of which have remained largely unstudied to date. Indeed, the potential of differential sedimentation profiles in a single sample became apparent, as we were able to point to two previously unannotated ncRNAs in the phage (Fig. 11), whereas TSS mapping in ΦKZ (51) failed to predict such candidates. To put this into perspective, a mere 21 ncRNAs have been described in phages to date (97); hence, Grad-seq offers an orthogonal approach for the identification of RNA processing sites and ncRNAs.

MATERIALS AND METHODS

Cell preparation, lysis, and gradient sedimentation. *Pseudomonas aeruginosa* strain PAO1 (JVS-11761, German Collection of Microorganisms and Cell cultures GmbH; DSM 22644, BacDive identifier [ID] 12801, NCBI tax-ID 208964) (see Table S2 in the supplemental material) was grown in 400 ml LB medium to an OD_{600} of 0.3 at 37°C. Optionally, the cells were infected with phage ΦKZ at a multiplicity of infection (MOI) of 15 to ensure immediate infection of the entire culture. To ensure that infected cell culture was in the early infection phase, the infected culture was mixed and incubated for 5 min at room temperature without shaking, followed by incubation at 37°C for 5 min with shaking, as described previously (30). The culture was cooled rapidly on ice, and the cells were pelleted at 6,000 × *g* for 15 min at 4°C and washed three times with ice-cold TBS (20 mM Tris-HCl [pH 7.4], 150 mM NaCl).

The gradient analysis was performed as published (22), with minor modifications. Cells were resuspended in 0.5 ml lysis buffer (20 mM Tris-HCl [pH 7.5], 150 mM KCl, 1 mM $MgCl_2$, 1 mM dithiothreitol [DTT], 1 mM phenylmethylsulfonyl fluoride [PMSF], 0.2% [vol/vol] Triton X-100, 20 U/ml DNase I [Thermo Fisher Scientific], 200 U/ml SUPERase-IN [Life Technologies]) and one volume of 0.1-mm glass beads. Lysis was obtained by vortexing this mix for 30 s, followed by 15 s of cooling on ice. This process was repeated 10 times, and the lysate was cleared at 12,000 × *g* for 10 min at 4°C. The supernatant was used for SDS-PAGE analysis and RNA preparation by TRIzol (Thermo Fischer Scientific). Aliquots of 180 μl supernatant were layered on a linear 10% to 40% (wt/vol) glycerol gradient and were sedimented in a SW40Ti rotor at 100,000 × *g* for 17 h at 4°C. The gradient was fractionated in 590-μl fractions, and the absorption was determined at 260 nm. Protein samples for SDS-PAGE were prepared for each individual fraction and analyzed as previously described (22). A 0.5-ml volume of each fraction was used for RNA

isolation by addition of 1% SDS and, subsequently, 600 μl acidic phenol-chloroform-isoamyl alcohol (PCI; Carl Roth). Samples were vortexed extensively, and the phases were separated by centrifugation. The upper aqueous layer was extracted repeatedly with chloroform. The aqueous layer was selected and precipitated by three volumes ice-cold ethanol with 0.3 M sodium acetate (NaOAc; pH 6.5). GlycoBlue (1 μl) (Thermo Fischer Scientific) was added as tracer. After overnight storage at −20°C, the precipitated RNA was pelleted, washed with 70% ethanol, dried, and dissolved in nuclease-free water for by Northern blotting analysis, as previously described (98) with oligomers listed in Table S2.

RNA sequencing. RNA samples from the gradient factions of naive or ΦKZ-infected bacteria were diluted 1:10 with nuclease-free water, and 10 μl of the dilution was mixed with 10 μl of 1:100 diluted ERCC RNA spike-in mix 1 (Thermo Fischer Scientific). This mix was used as an external RNA control for read normalization and to determine the dynamic range in sequencing, as suggested in best practice guidelines by the External RNA Controls Consortium (99). RNA-sequencing libraries were prepared by VERTIS Biotechnologie AG (Freising, Germany) as previously described (29). In essence, RNA samples were fragmented by ultrasound (four pulses of 30 s at 4°C) followed by 3′ adapter ligation. The 3′ adapter served as primer, and synthesis of the first-strand cDNA was performed using M-MLV reverse transcriptase. After purification, a 5′ Illumina TruSeq sequencing adapter was ligated to the end of the antisense cDNA. The resulting cDNA was PCR amplified to approximately 10 to 20 ng/μl using a high-fidelity DNA polymerase and purified with the Agencourt AMPure XP kit (Beckman Coulter Genomics). The cDNA samples were pooled based on the ratios according to the RNA concentrations of the input samples, and a size range of 200 to 550 bp was eluted from a preparative agarose gel. This size-selected cDNA pool was finally subjected to sequencing on an Illumina NextSeq 500 system using a 75-nt single-end read length.

Mass spectrometry. The nanoscale liquid chromatography tandem mass spectrometry (nanoLC-MS/MS) analysis was performed as previously described (29). Protein samples diluted in 1.25× protein loading buffer were homogenized by ultrasound (five cycles of 30 s on followed by 30 s off, high power at 4°C with a Bioruptor Plus; Diagenode). Insoluble material was removed by pelleting at full speed. A 20-μl sample of the cleared protein was mixed with 10 μl of UPS2 spike-in (Sigma-Aldrich) and diluted in 250 μl of 1.25× protein loading buffer. The samples were subsequently reduced in 50 mM DTT for 10 min at 70°C and alkylated with 120 mM iodoacetamide for 20 min at room temperature in the dark. The proteins were precipitated in four volumes of acetone overnight at −20°C. Pellets were washed four times with ice-cold acetone and dissolved in 50 μl of 8 M urea and 100 mM ammonium bicarbonate. Digestion of the proteins was performed by 0.25 μg Lys-C (Wako) for 2 h at 30°C, followed by dilution to 2 M urea by addition of 3 volumes 100 mM ammonium bicarbonate, pH 8, and overnight digestion with 0.25 μg trypsin at 37°C.

Peptides were purified through C_{18} Stage tips (100). Each Stage tip was prepared with three disks of C_{18} Empore SPE disks (3M) in a 200-μl pipette tip. Peptides were eluted with 60% acetonitrile-0.3% formic acid, lyophilized in a laboratory freeze-dryer (Christ), and stored at −20°C. Prior to nanoLC-MS/MS, the peptides were dissolved in 2% acetonitrile-0.1% formic acid.

NanoLC-MS/MS analysis. NanoLC-MS/MS analysis was performed as previously described (29) with an Orbitrap Fusion (Thermo Fisher Scientific) equipped with a PicoView ion source (New Objective) and coupled to an EASY-nLC 1000 (Thermo Fisher Scientific). Peptides were loaded on capillary columns (PicoFrit, 30 cm, 150-μm inside diameter; New Objective) self-packed with ReproSil-Pur 120 C_{18}-AQ, 1.9 μm (Dr. Maisch), and separated with a 140-min linear gradient from 3% to 40% acetonitrile and 0.1% formic acid at a flow rate of 500 nl/min.

Both MS and MS/MS scans were acquired in the Orbitrap analyzer with a resolution of 60,000 for MS scans and 15,000 for MS/MS scans. High-energy collisional dissociation (HCD) fragmentation with 35% normalized collision energy was applied. A Top Speed data-dependent MS/MS method with a fixed cycle time of 3 s was used. Dynamic exclusion was applied with a repeat count of 1 and an exclusion duration of 60 s. Precursors that were singly charged were excluded from selection. Minimum signal threshold for precursor selection was set to 50,000. Predictive automatic gain control (AGC) was used with a target value of 2×105 for MS scans and 5×104 for MS/MS scans. EASY-IC was used for internal calibration.

Grad-seq RNA data analysis. Reads were mapped to the *Pseudomonas* and ΦKZ reference sequences (NC_002516 and NC_004629, respectively) using the READemption align function (READemption version 0.4.3, [101]). Approximately ~96% of reads were aligned; for details, see the statistics files in the READemption analysis folder. Coverage wig-files were generated with the coverage function, and read allocation to genomic features was quantified by the gene_quanti function (gff files are supplied in the READemption analysis folder, Zenodo 4024332). Annotation of 3′/5′ UTRs was used from our parallel study and sRNAs from PseudoCAP (42), and manually annotated transcripts were added. Sequencing coverages were visualized in the Integrative Genomics Viewer (IGV; Broad Institute [102]) based on uniquely mapped reads and normalized to the total number of aligned reads.

Grad-seq MS data analysis. Raw MS data files were analyzed with MaxQuant version 1.6.2.2 (103). Database search was performed with Andromeda, which is integrated in the utilized version of MaxQuant. The search was performed against the UniProt *Pseudomonas aeruginosa* UP000002438 (strain PAO1), the ΦKZ proteome UP000002098 (37), and a database containing the proteins of the UPS2 proteomic standard. In addition, a database containing common contaminants was used. The search was performed with tryptic cleavage specificity with three allowed missed cleavages. Protein identification was under the control of the false-discovery rate (FDR; 1% on protein and peptide level). In addition to MaxQuant default settings, the search was additionally performed for the following variable modifications: protein N-terminal acetylation, glutamine to pyro-glutamic acid formation (N-terminal glutamine),

and oxidation (methionine). Carbamidomethyl (cysteine) was set as a fixed modification. For protein quantitation, the intensity-based absolute quantification (iBAQ) intensities were used (104). Proteins that could not be distinguished by peptides were listed individually.

Normalization and dose-response curves. Relative protein abundance in gradient fractions were calculated by iBAQ, as described previously (75). Relative protein abundance was estimated by correcting for alterations in digestion and C_{18} purification in fractions by normalization to human albumin (Table S1, norm. to spike-in, P02768ups|ALBU_HUMAN_UPS serum albumin, chain 26 to 609, Fig. S1A to C) that was spiked-in as part of the UPS2 standard (Sigma-Aldrich). We selected albumin for normalization because of the highest number of recovered peptides (105). In bar diagram representation, the abundances for each individual protein were transformed into distributions across the gradient by dividing the abundance in each fraction by the maximal abundance across the gradient (Table S1, norm. to max.). For visualization purposes of differential sedimentation representation, the *y* axes of individual profiles were scaled to the largest value in both represented gradients. For RNAs, basically the same approach was used with the ERCC-0130 spike-in, as all spike-in RNAs were well correlated in sample-wise quantification. Based on the corrected quantification values, we setup a dose-response curve plotting the measured relative abundance versus the input abundance (Fig. S1D to F). The linear range of recovery was determined for proteins being $\log_{10}$ iBAQ of $>$7.5 and for $\log_{10}$ RNA levels of $>$1.5. All proteins and RNAs that were recovered below the threshold were neglected, representing 614 proteins (Fig. S1B) and 2,182 RNAs (Fig. S1E).

Oligonucleotide probe labeling and Northern blotting. Oligonucleotides were radioactively labeled at 5′-OH with [γ-^{32}P]ATP by the T4-polynucleotide kinase, as reported previously (75). Northern probing was performed as previously reported (98).

Data availability. MS data are accessible at the ProteomeXchange consortium (106) via the PRIDE partner repository (107) with the data set identifier PXD021359. Raw data after MaxQuant and sequencing analysis are listed in Table S1. Sequencing raw FASTQ and analyzed WIG and TDF coverage files are accessible at Gene Expression Omnibus (GEO [108]) with the accession number GSE157708. The code for the Grad-seq browser is deposited at Zenodo (https://zenodo.org/record/3955585). The Grad-seq browser is online, accessible at https://helmholtz-hiri.de/en/datasets/gradseqpao1. READemption 0.4.5 is deposited at Zenodo 1134354 (https://zenodo.org/record/1134354). The READemption analysis folder is deposited at Zenodo 4024332 (https://zenodo.org/record/4024332).

SUPPLEMENTAL MATERIAL

Supplemental material is available online only.

FIG S1, PDF file, 0.2 MB.

FIG S2, PDF file, 0.4 MB.

FIG S3, PDF file, 0.2 MB.

FIG S4, PDF file, 0.4 MB.

FIG S5, PDF file, 1.2 MB.

FIG S6, PDF file, 0.2 MB.

FIG S7, PDF file, 0.2 MB.

FIG S8, PDF file, 1.7 MB.

TABLE S1, XLSX file, 2.9 MB.

TABLE S2, XLSX file, 0.1 MB.

ACKNOWLEDGMENTS

We thank Barbara Plaschke for technical assistance and Stephanie Lamer, Andreas Schlosser, Jens Hör, Lars Barquist, Konrad Förstner, and Silvia di Giorgio for helpful discussions about experiments and data analysis.

This work was supported by the Helmholtz Institute for RNA-based Infection Research (HIRI) with a seed grant through funds from the Bavarian Ministry of Economic Affairs and Media, Energy and Technology (grant allocation no. 0703/68674/5/2017 and 0703/89374/3/2017). This work was also supported by a Gottfried Wilhelm Leibniz award (DFG Vo875/18). L.W. holds a predoctoral scholarship from FWO-fundamental research (11D8920N). The manuscript was supported by funding from the European Research Council (ERC) under the European Union's Horizon 2020 research and innovation program (grant agreement No. 819800) awarded to R.L.

L.W., M.G., and J.V. designed and performed experiments. M.G. analyzed the Grad-seq data, carried out bioinformatics analyses, and generated figures for the manuscript. M.G. and J.V. wrote the manuscript with input from all authors. J.V. supervised and guided the project and interpreted Grad-seq data. All authors approved the final version.

We declare no competing interests.

REFERENCES

1. Jernigan JA, Hatfield KM, Wolford H, Nelson RE, Olubajo B, Reddy SC, McCarthy N, Paul P, McDonald LC, Kallen A, Fiore A, Craig M, Baggs J. 2020. Multidrug-resistant bacterial infections in U.S. hospitalized patients, 2012–2017. N Engl J Med 382:1309–1319. https://doi.org/10.1056/NEJMoa1914433.
2. Mulani MS, Kamble EE, Kumkar SN, Tawre MS, Pardesi KR. 2019. Emerging strategies to combat ESKAPE pathogens in the era of antimicrobial resistance: a review. Front Microbiol 10:539. https://doi.org/10.3389/fmicb.2019.00539.
3. Lamut A, Peterlin Masic L, Kikelj D, Tomasic T. 2019. Efflux pump inhibitors of clinically relevant multidrug resistant bacteria. Med Res Rev 39:2460–2504. https://doi.org/10.1002/med.21591.
4. Stover CK, Pham XQ, Erwin AL, Mizoguchi SD, Warrener P, Hickey MJ, Brinkman FSL, Hufnagle WO, Kowalik DJ, Lagrou M, Garber RL, Goltry L, Tolentino E, Westbrock-Wadman S, Yuan Y, Brody LL, Coulter SN, Folger KR, Kas A, Larbig K, Lim R, Smith K, Spencer D, Wong GKS, Wu Z, Paulsen IT, Reizer J, Saier MH, Hancock REW, Lory S, Olson MV. 2000. Complete genome sequence of *Pseudomonas aeruginosa* PAO1, an opportunistic pathogen. Nature 406:959–964. https://doi.org/10.1038/35023079.
5. Grenga L, Little RH, Malone JG. 2017. Quick change: post-transcriptional regulation in *Pseudomonas*. FEMS Microbiol Lett 364:fnx125. https://doi.org/10.1093/femsle/fnx125.
6. Holmqvist E, Vogel J. 2018. RNA-binding proteins in bacteria. Nat Rev Microbiol 16:601–615. https://doi.org/10.1038/s41579-018-0049-5.
7. Sonnleitner E, Schuster M, Sorger-Domenigg T, Greenberg EP, Bläsi U. 2006. Hfq-dependent alterations of the transcriptome profile and effects on quorum sensing in *Pseudomonas aeruginosa*. Mol Microbiol 59:1542–1558. https://doi.org/10.1111/j.1365-2958.2006.05032.x.
8. Chihara K, Bischler T, Barquist L, Monzon VA, Noda N, Vogel J, Tsuneda S. 2019. Conditional Hfq association with small noncoding RNAs in *Pseudomonas aeruginosa* revealed through comparative UV cross-linking immunoprecipitation followed by high-throughput sequencing. mSystems 4:e00590-19. https://doi.org/10.1128/mSystems.00590-19.
9. Kambara TK, Ramsey KM, Dove SL. 2018. Pervasive targeting of nascent transcripts by Hfq. Cell Rep 23:1543–1552. https://doi.org/10.1016/j.celrep.2018.03.134.
10. Zhang Y-F, Han K, Chandler CE, Tjaden B, Ernst RK, Lory S. 2017. Probing the sRNA regulatory landscape of *P aeruginosa*: post-transcriptional control of determinants of pathogenicity and antibiotic susceptibility. Mol Microbiol 106:919–937. https://doi.org/10.1111/mmi.13857.
11. Han K, Tjaden B, Lory S. 2016. GRIL-seq provides a method for identifying direct targets of bacterial small regulatory RNA by *in vivo* proximity ligation. Nat Microbiol 2:16239. https://doi.org/10.1038/nmicrobiol.2016.239.
12. Pei XY, Dendooven T, Sonnleitner E, Chen S, Bläsi U, Luisi BF. 2019. Architectural principles for Hfq/Crc-mediated regulation of gene expression. Elife 8:e43158. https://doi.org/10.7554/eLife.43158.
13. Sonnleitner E, Wulf A, Campagne S, Pei X-Y, Wolfinger MT, Forlani G, Prindl K, Abdou L, Resch A, Allain FH-T, Luisi BF, Urlaub H, Bläsi U. 2018. Interplay between the catabolite repression control protein Crc, Hfq and RNA in Hfq-dependent translational regulation in *Pseudomonas aeruginosa*. Nucleic Acids Res 46:1470–1485. https://doi.org/10.1093/nar/gkx1245.
14. Marden JN, Diaz MR, Walton WG, Gode CJ, Betts L, Urbanowski ML, Redinbo MR, Yahr TL, Wolfgang MC. 2013. An unusual CsrA family member operates in series with RsmA to amplify posttranscriptional responses in *Pseudomonas aeruginosa*. Proc Natl Acad Sci U S A 110:15055–15060. https://doi.org/10.1073/pnas.1307217110.
15. Morris ER, Hall G, Li C, Heeb S, Kulkarni RV, Lovelock L, Silistre H, Messina M, Cámara M, Emsley J, Williams P, Searle MS. 2013. Structural rearrangement in an RsmA/CsrA ortholog of *Pseudomonas aeruginosa* creates a dimeric RNA-binding protein, RsmN. Structure 21:1659–1671. https://doi.org/10.1016/j.str.2013.07.007.
16. Pessi G, Williams F, Hindle Z, Heurlier K, Holden MT, Cámara M, Haas D, Williams P. 2001. The global posttranscriptional regulator RsmA modulates production of virulence determinants and *N*-acylhomoserine lactones in *Pseudomonas aeruginosa*. J Bacteriol 183:6676–6683. https://doi.org/10.1128/JB.183.22.6676-6683.2001.
17. Chihara K, Barquist L, Takasugi K, Noda N, Tsuneda S. 25 August 2020. Global identification of RsmA/N binding sites in *Pseudomonas aeruginosa* by *in vivo* UV CLIP-seq. bioRxiv https://doi.org/10.1101/2020.08.24.265819.
18. Romero M, Silistre H, Lovelock L, Wright VJ, Chan K-G, Hong K-W, Williams P, Cámara M, Heeb S. 2018. Genome-wide mapping of the RNA targets of the *Pseudomonas aeruginosa* riboregulatory protein RsmN. Nucleic Acids Res 46:6823–6840. https://doi.org/10.1093/nar/gky324.
19. Gebhardt MJ, Kambara TK, Ramsey KM, Dove SL. 2020. Widespread targeting of nascent transcripts by RsmA in *Pseudomonas aeruginosa*. Proc Natl Acad Sci U S A 117:10520–10529. https://doi.org/10.1073/pnas.1917587117.
20. Holmqvist E, Li L, Bischler T, Barquist L, Vogel J. 2018. Global maps of ProQ binding *in vivo* reveal target recognition via RNA structure and stability control at mRNA 3' ends. Mol Cell 70:971–982. https://doi.org/10.1016/j.molcel.2018.04.017.
21. Bauriedl S, Gerovac M, Heidrich N, Bischler T, Barquist L, Vogel J, Schoen C. 2020. The minimal meningococcal ProQ protein has an intrinsic capacity for structure-based global RNA recognition. Nat Commun 11:2823. https://doi.org/10.1038/s41467-020-16650-6.
22. Smirnov A, Forstner KU, Holmqvist E, Otto A, Gunster R, Becher D, Reinhardt R, Vogel J. 2016. Grad-seq guides the discovery of ProQ as a major small RNA-binding protein. Proc Natl Acad Sci U S A 113:11591–-11596. https://doi.org/10.1073/pnas.1609981113.
23. Melamed S, Adams PP, Zhang A, Zhang H, Storz G. 2020. RNA-RNA interactomes of ProQ and Hfq reveal overlapping and competing roles. Mol Cell 77:411–425. https://doi.org/10.1016/j.molcel.2019.10.022.
24. Westermann AJ, Venturini E, Sellin ME, Förstner KU, Hardt W-D, Vogel J. 2019. The major RNA-binding protein ProQ impacts virulence gene expression in *Salmonella enterica* serovar Typhimurium. mBio 10:e02504-18. https://doi.org/10.1128/mBio.02504-18.
25. Olejniczak M, Storz G. 2017. ProQ/FinO-domain proteins: another ubiquitous family of RNA matchmakers? Mol Microbiol 104:905–915. https://doi.org/10.1111/mmi.13679.
26. Michaux C, Holmqvist E, Vasicek E, Sharan M, Barquist L, Westermann AJ, Gunn JS, Vogel J. 2017. RNA target profiles direct the discovery of virulence functions for the cold-shock proteins CspC and CspE. Proc Natl Acad Sci U S A 114:6824–6829. https://doi.org/10.1073/pnas.1620772114.
27. Smith T, Villanueva E, Queiroz RML, Dawson CS, Elzek M, Urdaneta EC, Willis AE, Beckmann BM, Krijgsveld J, Lilley KS. 2020. Organic phase separation opens up new opportunities to interrogate the RNA-binding proteome. Curr Opin Chem Biol 54:70–75. https://doi.org/10.1016/j.cbpa.2020.01.009.
28. Hör J, Di Giorgio S, Gerovac M, Venturini E, Förstner KU, Vogel J. 2020. Grad-seq shines light on unrecognized RNA and protein complexes in the model bacterium *Escherichia coli*. Nucleic Acids Res 48:9301–9319. https://doi.org/10.1093/nar/gkaa676.
29. Hör J, Garriss G, Di Giorgio S, Hack L-M, Vanselow JT, Förstner KU, Schlosser A, Henriques-Normark B, Vogel J. 2020. Grad-seq in a Gram-positive bacterium reveals exonucleolytic sRNA activation in competence control. EMBO J 39:e103852. https://doi.org/10.15252/embj.2019103852.
30. Ceyssens P-J, Minakhin L, Van den Bossche A, Yakunina M, Klimuk E, Blasdel B, De Smet J, Noben J-P, Bläsi U, Severinov K, Lavigne R. 2014. Development of giant bacteriophage ϕKZ is independent of the host transcription apparatus. J Virol 88:10501–10510. https://doi.org/10.1128/JVI.01347-14.
31. Kavaliauskas D, Nissen P, Knudsen CR. 2012. The busiest of all ribosomal assistants: elongation factor Tu. Biochemistry 51:2642–2651. https://doi.org/10.1021/bi300077s.
32. Huter P, Müller C, Arenz S, Beckert B, Wilson DN. 2017. Structural basis for ribosome rescue in bacteria. Trends Biochem Sci 42:669–680. https://doi.org/10.1016/j.tibs.2017.05.009.
33. Vogel DW, Hartmann RK, Struck JC, Ulbrich N, Erdmann VA. 1987. The sequence of the 6S RNA gene of *Pseudomonas aeruginosa*. Nucleic Acids Res 15:4583–4591. https://doi.org/10.1093/nar/15.11.4583.
34. Wassarman KM, Storz G. 2000. 6S RNA regulates *E. coli* RNA polymerase activity. Cell 101:613–623. https://doi.org/10.1016/s0092-8674(00)80873-9.
35. Wassarman KM, Saecker RM. 2006. Synthesis-mediated release of a small RNA inhibitor of RNA polymerase. Science 314:1601–1603. https://doi.org/10.1126/science.1134830.
36. Gildehaus N, Neußer T, Wurm R, Wagner R. 2007. Studies on the function of the riboregulator 6S RNA from *E. coli*: RNA polymerase binding, inhibition of *in vitro* transcription and synthesis of RNA-directed *de novo* transcripts. Nucleic Acids Res 35:1885–1896. https://doi.org/10.1093/nar/gkm085.
37. UniProt Consortium. 2018. UniProt: a worldwide hub of protein knowledge. Nucleic Acids Res 47:D506–D515. https://doi.org/10.1093/nar/gky1049.
38. Lee J, Oh S, Bhattacharya S, Zhang Y, Florens L, Washburn MP, Workman

JL. 2 June 2020. The plasticity of the pyruvate dehydrogenase complex confers a labile structure that is associated with its catalytic activity. bioRxiv https://doi.org/10.1101/2020.06.02.130369.
39. Joyce MA, Fraser ME, James MNG, Bridger WA, Wolodko WT. 2000. ADP-binding site of *Escherichia coli* succinyl-CoA synthetase revealed by X-ray crystallography. Biochemistry 39:17–25. https://doi.org/10.1021/bi991696f.
40. Saikawa N, Akiyama Y, Ito K. 2004. FtsH exists as an exceptionally large complex containing HflKC in the plasma membrane of *Escherichia coli*. J Struct Biol 146:123–129. https://doi.org/10.1016/j.jsb.2003.09.020.
41. Dötsch A, Eckweiler D, Schniederjans M, Zimmermann A, Jensen V, Scharfe M, Geffers R, Häussler S. 2012. The *Pseudomonas aeruginosa* transcriptome in planktonic cultures and static biofilms using RNA sequencing. PLoS One 7:e31092. https://doi.org/10.1371/journal.pone.0031092.
42. Winsor GL, Griffiths EJ, Lo R, Dhillon BK, Shay JA, Brinkman Fiona SL. 2016. Enhanced annotations and features for comparing thousands of *Pseudomonas* genomes in the *Pseudomonas* genome database. Nucleic Acids Res 44:D646–D653. https://doi.org/10.1093/nar/gkv1227.
43. Hör J, Matera G, Vogel J, Gottesman S, Storz G. 2020. Trans-acting small RNAs and their effects on gene expression in *Escherichia coli* and *Salmonella enterica*. EcoSal Plus 2020:ESP-0030-2019. https://doi.org/10.1128/ecosalplus.ESP-0030-2019.
44. Papenfort K, Förstner KU, Cong J-P, Sharma CM, Bassler BL. 2015. Differential RNA-seq of *Vibrio cholerae* identifies the VqmR small RNA as a regulator of biofilm formation. Proc Natl Acad Sci U S A 112:E766–E775. https://doi.org/10.1073/pnas.1500203112.
45. Gómez-Lozano M, Marvig RL, Molin S, Long KS. 2012. Genome-wide identification of novel small RNAs in *Pseudomonas aeruginosa*. Environ Microbiol 14:2006–2016. https://doi.org/10.1111/j.1462-2920.2012.02759.x.
46. Ferrara S, Brugnoli M, De Bonis A, Righetti F, Delvillani F, Dehò G, Horner D, Briani F, Bertoni G. 2012. Comparative profiling of *Pseudomonas aeruginosa* strains reveals differential expression of novel unique and conserved small RNAs. PLoS One 7:e36553. https://doi.org/10.1371/journal.pone.0036553.
47. Wagner EGH, Romby P. 2015. Small RNAs in bacteria and archaea: who they are, what they do, and how they do it. Adv Genet 90:133–208. https://doi.org/10.1016/bs.adgen.2015.05.001.
48. Chakravarty S, Massé E. 2019. RNA-dependent regulation of virulence in pathogenic bacteria. Front Cell Infect Microbiol 9:337. https://doi.org/10.3389/fcimb.2019.00337.
49. Miyakoshi M, Chao Y, Vogel J. 2015. Regulatory small RNAs from the 3′ regions of bacterial mRNAs. Curr Opin Microbiol 24:132–139. https://doi.org/10.1016/j.mib.2015.01.013.
50. Adams PP, Storz G. 2020. Prevalence of small base-pairing RNAs derived from diverse genomic loci. Biochim Biophys Acta Gene Regul Mech 1863:194524. https://doi.org/10.1016/j.bbagrm.2020.194524.
51. Wicke L, Ponath F, Coppens L, Gerovac M, Lavigne R, Vogel J. 25 October 2020. Introducing differential RNA-seq mapping to track the early infection phase for *Pseudomonas* phage ΦKZ. RNA Biol https://doi.org/10.1080/15476286.2020.1827785.
52. Wurtzel O, Yoder-Himes DR, Han K, Dandekar AA, Edelheit S, Greenberg EP, Sorek R, Lory S. 2012. The single-nucleotide resolution transcriptome of *Pseudomonas aeruginosa* grown in body temperature. PLoS Pathog 8:e1002945. https://doi.org/10.1371/journal.ppat.1002945.
53. Gill EE, Chan LS, Winsor GL, Dobson N, Lo R, Ho Sui SJ, Dhillon BK, Taylor PK, Shrestha R, Spencer C, Hancock REW, Unrau PJ, Brinkman FSL. 2018. High-throughput detection of RNA processing in bacteria. BMC Genomics 19:223. https://doi.org/10.1186/s12864-018-4538-8.
54. Chao Y, Vogel J. 2016. The 3′UTR-derived small RNA provides the regulatory noncoding arm of the inner membrane stress response. Mol Cell 61:352–363. https://doi.org/10.1016/j.molcel.2015.12.023.
55. Thomason MK, Voichek M, Dar D, Addis V, Fitzgerald D, Gottesman S, Sorek R, Greenberg EP. 2019. A *rhlI* 5′ UTR-derived sRNA regulates RhlR-dependent quorum sensing in *Pseudomonas aeruginosa*. mBio 10:e02253-19. https://doi.org/10.1128/mBio.02253-19.
56. Wright PR, Georg J, Mann M, Sorescu DA, Richter AS, Lott S, Kleinkauf R, Hess WR, Backofen R. 2014. CopraRNA and IntaRNA: predicting small RNA targets, networks and interaction domains. Nucleic Acids Res 42:W119–W123. https://doi.org/10.1093/nar/gku359.
57. Sonnleitner E, Gonzalez N, Sorger-Domenigg T, Heeb S, Richter AS, Backofen R, Williams P, Hüttenhofer A, Haas D, Bläsi U. 2011. The small RNA PhrS stimulates synthesis of the *Pseudomonas aeruginosa* quinolone signal. Mol Microbiol 80:868–885. https://doi.org/10.1111/j.1365-2958.2011.07620.x.
58. Sonnleitner E, Bläsi U. 2014. Regulation of Hfq by the RNA CrcZ in *Pseudomonas aeruginosa* carbon catabolite repression. PLoS Genet 10:e1004440. https://doi.org/10.1371/journal.pgen.1004440.
59. Brencic A, Lory S. 2009. Determination of the regulon and identification of novel mRNA targets of *Pseudomonas aeruginosa* RsmA. Mol Microbiol 72:612–632. https://doi.org/10.1111/j.1365-2958.2009.06670.x.
60. Duss O, Michel E, Yulikov M, Schubert M, Jeschke G, Allain FHT. 2014. Structural basis of the non-coding RNA RsmZ acting as a protein sponge. Nature 509:588–592. https://doi.org/10.1038/nature13271.
61. El-Gebali S, Mistry J, Bateman A, Eddy SR, Luciani A, Potter SC, Qureshi M, Richardson LJ, Salazar GA, Smart A, Sonnhammer ELL, Hirsh L, Paladin L, Piovesan D, Tosatto SE, Finn RD. 2019. The Pfam protein families database in 2019. Nucleic Acids Res 47:D427–D432. https://doi.org/10.1093/nar/gky995.
62. Djapgne L, Panja S, Brewer LK, Gans JH, Kane MA, Woodson SA, Oglesby-Sherrouse AG. 2018. The *Pseudomonas aeruginosa* PrrF1 and PrrF2 small regulatory RNAs promote 2-alkyl-4-quinolone production through redundant regulation of the *antR* mRNA. J Bacteriol 200:e00704-17. https://doi.org/10.1128/JB.00704-17.
63. Sonnleitner E, Sorger-Domenigg T, Madej MJ, Findeiss S, Hackermüller J, Hüttenhofer A, Stadler PF, Bläsi U, Moll I. 2008. Detection of small RNAs in *Pseudomonas aeruginosa* by RNomics and structure-based bioinformatic tools. Microbiology (Reading) 154:3175–3187. https://doi.org/10.1099/mic.0.2008/019703-0.
64. Gómez Lozano M. 2013. Genome-wide identification of novel small RNAs in Pseudomonas aeruginosa. Novo Nordisk Foundation Center for Biosustainability, Technical University of Denmark, Lyngby, Denmark.
65. Weaver J, Mohammad F, Buskirk AR, Storz G. 2019. Identifying small proteins by ribosome profiling with stalled initiation complexes. mBio 10:e02819-18. https://doi.org/10.1128/mBio.02819-18.
66. Grady SL, Malfatti SA, Gunasekera TS, Dalley BK, Lyman MG, Striebich RC, Mayhew MB, Zhou CL, Ruiz ON, Dugan LC. 2017. A comprehensive multi-omics approach uncovers adaptations for growth and survival of *Pseudomonas aeruginosa* on *n*-alkanes. BMC Genomics 18:334–334. https://doi.org/10.1186/s12864-017-3708-4.
67. Mesyanzhinov VV, Robben J, Grymonprez B, Kostyuchenko VA, Bourkaltseva MV, Sykilinda NN, Krylov VN, Volckaert G. 2002. The genome of bacteriophage ϕKZ of *Pseudomonas aeruginosa*. J Mol Biol 317:1–19. https://doi.org/10.1006/jmbi.2001.5396.
68. De Smet J, Hendrix H, Blasdel BG, Danis-Wlodarczyk K, Lavigne R. 2017. *Pseudomonas* predators: understanding and exploiting phage–host interactions. Nat Rev Microbiol 15:517–530. https://doi.org/10.1038/nrmicro.2017.61.
69. Mendoza SD, Nieweglowska ES, Govindarajan S, Leon LM, Berry JD, Tiwari A, Chaikeeratisak V, Pogliano J, Agard DA, Bondy-Denomy J. 2020. A bacteriophage nucleus-like compartment shields DNA from CRISPR nucleases. Nature 577:244–248. https://doi.org/10.1038/s41586-019-1786-y.
70. Förster-Fromme K, Höschle B, Mack C, Bott M, Armbruster W, Jendrossek D. 2006. Identification of genes and proteins necessary for catabolism of acyclic terpenes and leucine/isovalerate in *Pseudomonas aeruginosa*. Appl Environ Microbiol 72:4819–4828. https://doi.org/10.1128/AEM.00853-06.
71. Falcone M, Ferrara S, Rossi E, Johansen HK, Molin S, Bertoni G. 2018. The small RNA ErsA of *Pseudomonas aeruginosa* contributes to biofilm development and motility through post-transcriptional modulation of AmrZ. Front Microbiol 9:238. https://doi.org/10.3389/fmicb.2018.00238.
72. Ferrara S, Carloni S, Fulco R, Falcone M, Macchi R, Bertoni G. 2015. Post-transcriptional regulation of the virulence-associated enzyme AlgC by the σ22-dependent small RNA ErsA of *Pseudomonas aeruginosa*. Environ Microbiol 17:199–214. https://doi.org/10.1111/1462-2920.12590.
73. Sonnleitner E, Pusic P, Wolfinger MT, Bläsi U. 2020. Distinctive regulation of carbapenem susceptibility in Pseudomonas aeruginosa by Hfq. Front Microbiol 11:11001. https://doi.org/10.3389/fmicb.2020.01001.
74. Khade P, Joseph S. 2010. Functional interactions by transfer RNAs in the ribosome. FEBS Lett 584:420–426. https://doi.org/10.1016/j.febslet.2009.11.034.
75. Gerovac M, El Mouali Y, Kuper J, Kisker C, Barquist L, Vogel J. 2020. Global discovery of bacterial RNA-binding proteins by RNase-sensitive gradient profiles reports a new FinO domain protein. RNA 26:1448–1463. https://doi.org/10.1261/rna.076992.120.
76. Pandey S, Gravel CM, Stockert OM, Wang CD, Hegner CL, LeBlanc H, Berry KE. 2020. Genetic identification of the functional surface for RNA binding by *Escherichia coli* ProQ. Nucleic Acids Res 48:4507–4520. https://doi.org/10.1093/nar/gkaa144.
77. De Smet J, Zimmermann M, Kogadeeva M, Ceyssens P-J, Vermaelen W, Blasdel B, Bin Jang H, Sauer U, Lavigne R. 2016. High coverage

metabolomics analysis reveals phage-specific alterations to *Pseudomonas aeruginosa* physiology during infection. ISME J 10:1823–1835. https://doi.org/10.1038/ismej.2016.3.
78. Van den Bossche A, Hardwick SW, Ceyssens P-J, Hendrix H, Voet M, Dendooven T, Bandyra KJ, De Maeyer M, Aertsen A, Noben J-P, Luisi BF, Lavigne R. 2016. Structural elucidation of a novel mechanism for the bacteriophage-based inhibition of the RNA degradosome. Elife 5:e16413. https://doi.org/10.7554/eLife.16413.
79. Uzan M, Miller ES. 2010. Post-transcriptional control by bacteriophage T4: mRNA decay and inhibition of translation initiation. Virol J 7:360–360. https://doi.org/10.1186/1743-422X-7-360.
80. Olins PO, Devine CS, Rangwala SH, Kavka KS. 1988. The T7 phage gene *10* leader RNA, a ribosome-binding site that dramatically enhances the expression of foreign genes in *Escherichia coli*. Gene 73:227–235. https://doi.org/10.1016/0378-1119(88)90329-0.
81. Kalousek S, Schrot G, Lubitz W, Bläsi U. 1994. Expression of the *Alcaligenes eutrophus phbA* gene in *Escherichia coli* using a positive selection vector based on phage Lambda lysis genes. J Biotechnol 33:15–19. https://doi.org/10.1016/0168-1656(94)90094-9.
82. Robertson ES, Nicholson AW. 1992. Phosphorylation of *Escherichia coli* translation initiation factors by the bacteriophage T7 protein kinase. Biochemistry 31:4822–4827. https://doi.org/10.1021/bi00135a012.
83. Robertson ES, Aggison LA, Nicholson AW. 1994. Phosphorylation of elongation factor G and ribosomal protein S6 in bacteriophage T7-infected *Escherichia coli*. Mol Microbiol 11:1045–1057. https://doi.org/10.1111/j.1365-2958.1994.tb00382.x.
84. Herrlich P, Rahmsdorf HJ, Pai SH, Schweigher M. 1974. Translational control induced by bacteriophage T7. Proc Natl Acad Sci U S A 71:1088–1092. https://doi.org/10.1073/pnas.71.4.1088.
85. Mizuno CM, Guyomar C, Roux S, Lavigne R, Rodriguez-Valera F, Sullivan MB, Gillet R, Forterre P, Krupovic M. 2019. Numerous cultivated and uncultivated viruses encode ribosomal proteins. Nat Commun 10:752. https://doi.org/10.1038/s41467-019-08672-6.
86. Al-Shayeb B, Sachdeva R, Chen L-X, Ward F, Munk P, Devoto A, Castelle CJ, Olm MR, Bouma-Gregson K, Amano Y, He C, Méheust R, Brooks B, Thomas A, Lavy A, Matheus-Carnevali P, Sun C, Goltsman DSA, Borton MA, Sharrar A, Jaffe AL, Nelson TC, Kantor R, Keren R, Lane KR, Farag IF, Lei S, Finstad K, Amundson R, Anantharaman K, Zhou J, Probst AJ, Power ME, Tringe SG, Li W-J, Wrighton K, Harrison S, Morowitz M, Relman DA, Doudna JA, Lehours A-C, Warren L, Cate JHD, Santini JM, Banfield JF. 2020. Clades of huge phages from across Earth's ecosystems. Nature 578:425–431. https://doi.org/10.1038/s41586-020-2007-4.
87. Millman A, Melamed S, Amitai G, Sorek R. 2020. Diversity and classification of cyclic-oligonucleotide-based anti-phage signalling systems. Nat Microbiol 5:1608–1615. https://doi.org/10.1038/s41564-020-0777-y.
88. Lin P, Pu Q, Wu Q, Zhou C, Wang B, Schettler J, Wang Z, Qin S, Gao P, Li R, Li G, Cheng Z, Lan L, Jiang J, Wu M. 2019. High-throughput screen reveals sRNAs regulating crRNA biogenesis by targeting CRISPR leader to repress Rho termination. Nature Commun 10:3728. https://doi.org/10.1038/s41467-019-11695-8.
89. Dendooven T, Lavigne R. 2019. Dip-a-dee-doo-dah: bacteriophage-mediated rescoring of a harmoniously orchestrated RNA metabolism. Annu Rev Virol 6:199–213. https://doi.org/10.1146/annurev-virology-092818-015644.
90. Okamoto K, Sugino Y, Nomura M. 1962. Synthesis and turnover of phage messenger RNA in *E. coli* infected with bacteriophage T4 in the presence of chloromycetin. J Mol Biol 5:527–534. https://doi.org/10.1016/S0022-2836(62)80126-0.
91. Dendooven T, Van den Bossche A, Hendrix H, Ceyssens P-J, Voet M, Bandyra KJ, De Maeyer M, Aertsen A, Noben J-P, Hardwick SW, Luisi BF, Lavigne R. 2017. Viral interference of the bacterial RNA metabolism machinery. RNA Biol 14:6–10. https://doi.org/10.1080/15476286.2016.1251003.
92. Jain C, Belasco JG. 1995. Autoregulation of RNase E synthesis in *Escherichia coli*. Nucleic Acids Symp Ser 1995:85–88.
93. Diwa A, Bricker AL, Jain C, Belasco JG. 2000. An evolutionarily conserved RNA stem–loop functions as a sensor that directs feedback regulation of RNase E gene expression. Genes Dev 14:1249–1260.
94. Schuck A, Diwa A, Belasco JG. 2009. RNase E autoregulates its synthesis in *Escherichia coli* by binding directly to a stem-loop in the rne 5′ untranslated region. Mol Microbiol 72:470–478. https://doi.org/10.1111/j.1365-2958.2009.06662.x.
95. Weinberg Z, Wang JX, Bogue J, Yang J, Corbino K, Moy RH, Breaker RR. 2010. Comparative genomics reveals 104 candidate structured RNAs from bacteria, archaea, and their metagenomes. Genome Biol 11:R31. https://doi.org/10.1186/gb-2010-11-3-r31.
96. Stazic D, Pekarski I, Kopf M, Lindell D, Steglich C. 2016. A novel strategy for exploitation of host RNase E activity by a marine cyanophage. Genetics 203:1149–1159. https://doi.org/10.1534/genetics.115.183475.
97. Bloch S, Lewandowska N, Węgrzyn G, Nejman-Faleńczyk B. 5 August 2020. Bacteriophages as sources of small non-coding RNA molecules. Plasmid https://doi.org/10.1016/j.plasmid.2020.102527.
98. Sharma CM, Papenfort K, Pernitzsch SR, Mollenkopf H-J, Hinton JCD, Vogel J. 2011. Pervasive post-transcriptional control of genes involved in amino acid metabolism by the Hfq-dependent GcvB small RNA. Mol Microbiol 81:1144–1165. https://doi.org/10.1111/j.1365-2958.2011.07751.x.
99. Baker SC, Bauer SR, Beyer RP, Brenton JD, Bromley B, Burrill J, Causton H, Conley MP, Elespuru R, Fero M, Foy C, Fuscoe J, Gao X, Gerhold DL, Gilles P, Goodsaid F, Guo X, Jackett J, Hockett RD, Ikonomi P, Irizarry RA, Kawasaki ES, Kaysser-Kranich T, Kerr K, Kiser G, Koch WH, Lee KY, Liu C, Liu L, Lucas A, Manohar CF, Miyada G, Modrusan Z, Parkes H, Puri RK, Reid L, Ryder TB, Salit M, Samaha RR, Scherf U, Sendera TJ, Setterquist RA, Shi L, Shippy R, Soriano JV, Wagar EA, Warrington JA, Williams M, Wilmer F, Wilson M, et al. 2005. The External RNA Controls Consortium: a progress report. Nat Methods 2:731–734. https://doi.org/10.1038/nmeth1005-731.
100. Rappsilber J, Ishihama Y, Mann M. 2003. Stop and go extraction tips for matrix-assisted laser desorption/ionization, nanoelectrospray, and LC/MS sample pretreatment in proteomics. Anal Chem 75:663–670. https://doi.org/10.1021/ac026117i.
101. Förstner KU, Vogel J, Sharma CM. 2014. READemption—a tool for the computational analysis of deep-sequencing–based transcriptome data. Bioinformatics 30:3421–3423. https://doi.org/10.1093/bioinformatics/btu533.
102. Robinson JT, Thorvaldsdóttir H, Winckler W, Guttman M, Lander ES, Getz G, Mesirov JP. 2011. Integrative genomics viewer. Nat Biotechnol 29:24–26. https://doi.org/10.1038/nbt.1754.
103. Cox J, Mann M. 2008. MaxQuant enables high peptide identification rates, individualized p.p.b.-range mass accuracies and proteome-wide protein quantification. Nat Biotechnol 26:1367–1372. https://doi.org/10.1038/nbt.1511.
104. Schwanhäusser B, Busse D, Li N, Dittmar G, Schuchhardt J, Wolf J, Chen W, Selbach M. 2011. Global quantification of mammalian gene expression control. Nature 473:337–342. https://doi.org/10.1038/nature10098.
105. Lott SC, Schäfer RA, Mann M, Backofen R, Hess WR, Voß B, Georg J. 2018. GLASSgo – automated and reliable detection of sRNA homologs from a single input sequence. Front Genetics 9:124. https://doi.org/10.3389/fgene.2018.00124.
106. Deutsch EW, Csordas A, Sun Z, Jarnuczak A, Perez-Riverol Y, Ternent T, Campbell DS, Bernal-Llinares M, Okuda S, Kawano S, Moritz RL, Carver JJ, Wang M, Ishihama Y, Bandeira N, Hermjakob H, Vizcaíno JA. 2017. The ProteomeXchange consortium in 2017: supporting the cultural change in proteomics public data deposition. Nucleic Acids Res 45:D1100–-D1106. https://doi.org/10.1093/nar/gkw936.
107. Perez-Riverol Y, Csordas A, Bai J, Bernal-Llinares M, Hewapathirana S, Kundu DJ, Inuganti A, Griss J, Mayer G, Eisenacher M, Pérez E, Uszkoreit J, Pfeuffer J, Sachsenberg T, Yılmaz Ş, Tiwary S, Cox J, Audain E, Walzer M, Jarnuczak AF, Ternent T, Brazma A, Vizcaíno JA. 2019. The PRIDE database and related tools and resources in 2019: improving support for quantification data. Nucleic Acids Res 47:D442–D450. https://doi.org/10.1093/nar/gky1106.
108. Edgar R, Domrachev M, Lash AE. 2002. Gene Expression Omnibus: NCBI gene expression and hybridization array data repository. Nucleic Acids Res 30:207–210. https://doi.org/10.1093/nar/30.1.207.
109. Zuker M. 2003. Mfold web server for nucleic acid folding and hybridization prediction. Nucleic Acids Res 31:3406–3415. https://doi.org/10.1093/nar/gkg595.